EUROPEAN COMMISSION

Community research

PAMINA
Performance Assessment Methodologies in Application to Guide the Development of the Safety Case

(Contract Number: FP6-036404)

Simulating the migration of repository gases through argillaceous rock by implementing the mechanism of pathway dilation into the code TOUGH2 (TOUGH2-PD) MILESTONE (N°:3.2.14)

Author(s): **Martin Navarro**

Gesellschaft für Anlagen- und Reaktorsicherheit (GRS) mbH

Date of issue of this report : **30/09/2009**

Start date of project : **01/10/2006** Duration : 36 Months

Project co-funded by the European Commission under the Euratom Research and Training Programme on Nuclear Energy within the Sixth Framework Programme (2002-2006)		
Dissemination Level		
PU	Public	X
RE	Restricted to a group specified by the partners of the [PAMINA] project	
CO	Confidential, only for partners of the [PAMINA] project	

Foreword

The work presented in this report was developed within the Integrated Project PAMINA: **P**erformance **A**ssessment **M**ethodologies **IN A**pplication to Guide the Development of the Safety Case. This project is part of the Sixth Framework Programme of the European Commission. It brings together 25 organisations from ten European countries and one EC Joint Research Centre in order to improve and harmonise methodologies and tools for demonstrating the safety of deep geological disposal of long-lived radioactive waste for different waste types, repository designs and geological environments. The results will be of interest to national waste management organisations, regulators and lay stakeholders.

The work is organised in four Research and Technology Development Components (RTDCs) and one additional component dealing with knowledge management and dissemination of knowledge:

- In RTDC 1 the aim is to evaluate the state of the art of methodologies and approaches needed for assessing the safety of deep geological disposal, on the basis of comprehensive review of international practice. This work includes the identification of any deficiencies in methods and tools.

- In RTDC 2 the aim is to establish a framework and methodology for the treatment of uncertainty during PA and safety case development. Guidance on, and examples of, good practice will be provided on the communication and treatment of different types of uncertainty, spatial variability, the development of probabilistic safety assessment tools, and techniques for sensitivity and uncertainty analysis.

- In RTDC 3 the aim is to develop methodologies and tools for integrated PA for various geological disposal concepts. This work includes the development of PA scenarios, of the PA approach to gas migration processes, of the PA approach to radionuclide source term modelling, and of safety and performance indicators.

- In RTDC 4 the aim is to conduct several benchmark exercises on specific processes, in which quantitative comparisons are made between approaches that rely on simplifying assumptions and models, and those that rely on complex models that take into account a more complete process conceptualization in space and time.

The work presented in this report was performed in the scope of RTDC 3.

All PAMINA reports can be downloaded from http://www.ip-pamina.eu.

Table of contents

1 Introduction

In a repository for radioactive wastes which is situated in indurated clay stone, gas pressures will rise if gas production rates exceed the outflow of gas from the repository by diffusion or visco-capillary flow. Well before gas pressures reach the minimal principal stress and macroscopic fractures form, gas may intrude into the rock by creating additional (secondary) pore space without causing any macro-fracturing. This mechanism has been called pathway dilation /HOR 96/ and may comprise growth and opening of microscopic pores or the connection of existing pores to the flow passages.

Pathway dilation is usually thought to take place above certain pressure thresholds but due to the small-scale heterogeneity of stresses and material properties there is probably no sharp transition to the dilated state. With regard to the materials present in deep geological repositories the process of pathway dilation has been investigated experimentally most intensively on bentonite /SWI 01, HOC 04/ but there is also experimental evidence for pathway dilation in indurated /MAR 05/ and plastic clays /MAZ 03/. Indications for pathway dilation are volumetric strains during gas entry and a non-linear dependency of gas flow on gas pressure.

Pathway dilation helps to maintain the integrity of natural and technical barriers by limiting gas pressures below thresholds for macro-fracturing. Although the hydraulic effects of macro-fracturing may be reversed due to a self-healing capability of the clay, uncertainties connected to the safety assessment can be considerably reduced if the absence of macro-fracturing can be shown. This can not be done in general but has to be demonstrated for each specific site and repository concept. The capability of pathway dilation to prevent macro-fracturing in the framework of a German repository concept has only been investigated in a simplified way so far /BFS 05/ and needs further research.

There is consensus, that the conventional two-phase flow theory which is based on an inert rock matrix and solely saturation-dependent capillary pressures is not able to describe the effect of pathway dilation in clay adequately /NEA 01, ROD 03/. Alternative modelling approaches therefore utilise coupled hydro-mechanical codes /HOC 04/ as well as modified two-phase flow codes with indirect consideration of mechanical processes /CAL 06, SEN 06, FIN 09/. The objective of modified two-phase flow models usually is to capture the dependency of phase mobility and storage capacity on rock dilation. Commonly, pressure-dependent intrinsic permeabilities /CAL 06, SEN 06, FIN 09/, capillary pressure functions /CAL 06/, and porosity-changes /FIN 09/ are introduced to achieve this objective. It is still a matter of research whether such approaches are sufficiently accurate for the assessment of repository safety and whether they are sufficiently physically substantiated. Pressure-dependent permeabilities for example may conflict with the observation of very low liquid mobility in gas injection tests.

In the PAMINA project, a conceptual model for pathway dilation was developed by GRS and implemented into the two-phase flow code TOUGH2 to account for dilation effects. The

modified code (called TOUGH2-PD) was used to investigate the influence of pathway dilation on the far-field transport of gas generated in a hypothetical German repository for radioactive wastes in clay stone, and to identify sensitive parameters.

2 Summary of code changes

2.1 TOUGH2-PD

In this chapter, a short overview over all code changes that have been carried out so far is given. The main features which have been added to the TOUGH2 code are based on the assumption that micro-cracks or other microscopic pores open if gas pressures exceed certain pressure thresholds. Additional pore space for the flow of the gas phase is created while the residual pore space remains more or less unaffected. It is assumed that the dilated gas pathways can be characterised by homogeneous hydraulic properties on a macroscopic scale (the scale of a grid element). Details of the conceptual model are given in section 3.3.1. The following features have been implemented:

- **Pressure-dependent porosity**. Due to pathway dilation the gas phase is thought to be mobile even if water can not be displaced (e.g. due to rigorous gas entry pressures or due to no-flow boundaries). To achieve this, additional pore space has to be created to accommodate the mobile gas phase or otherwise the gas phase would propagate with infinite pore velocity. For this reason, a pressure-dependent porosity has been implemented into the TOUGH2 code.

  In fact, a change of porosity is not of major importance in itself because the porosity changes considered here are very small compared to the total porosity of the rock. However, in media which are almost fully saturated, even a small addition of pore space occupied by a gas phase may significantly change the mobility of gas and the capacity of the rock to store a gas phase.

  Porosity increase was modelled separately from the porosity-change-feature of TOUGH2 which affects the fluxes but not the storage capacity of the rock. Due to the strong non-linearity of the relationships describing dilation behaviour, porosity and permeability are changed after completion of a time step in order to avoid convergence problems. To comply with the user-defined relationships between porosity and pressure and to guarantee mass conservation, porosities, pressures and saturations are changed after each time step. This is done by simulating isothermal compression or expansion of the pore space according to the thermodynamic processes implemented in the EOS7 module. It required an inverse formulation of some EOS-algorithms.

- **Pressure-dependent gas permeability.** An additional flux of the gas phase in the dilated pores is added to the flux in the non-deformed matrix. The additional flux follows Darcy's law using a pressure-dependent gas permeability for the dilated pores. This allows to use independent weighting schemes for the permeability of the dilated and of the unaffected pore space. Upstream weighting has been chosen for the permeability of the dilated pore space in order to attain an easy propagation of the dilation front.

- **Thresholds.** A scalar field for the minimal principal stress has been introduced to determine pressure thresholds for dilation relatively to the minimal principal stress. Different pressure thresholds may be defined for pore opening and closure.
- **Anisotropy.** A simple anisotropy model has been implemented into the TOUGH2 code. The user may define a number of micro-crack networks each with a specific dilation threshold, permeability-pressure and porosity-pressure-relationship and tensor for the anisotropy of permeability (Which does not imply that the dilated pores have to be cracks in reality).
- **Gas component.** The gas component of the EOS7 module has been changed from air to H_2. This includes changes to the molar mass, specific enthalpy, Henry-Isotherm and viscosity of the H_2-vapour mixture. Molar mass, specific enthalpy and Henry-Isotherm were taken from the EOS5-module which is why the Henry-Isotherm does not consider salinity yet. Viscosity of the gas phase is of minor importance in systems where a gas phase and a more viscous liquid phase are displaced simultaneously. Flow is then usually governed by the viscosity of the liquid. In the model presented here, the gas phase may migrate without displacing the liquid phase, so that more attention has to be paid to the viscosity of the gas phase. A new viscosity function for H_2-vapour mixtures has been implemented according to kinetic gas theory with data from /LAN 69/ and a pressure correction derived from the viscosity data used in the EOS5-module (note that viscosity depends only slightly on pressure).
- **Automatic time step control.** Using the automatic time step control of TOUGH2, time step widths can exceed ranges that have to be met to simulate the dilation-controlled transport processes appropriately (see section 4.2). The automatic time stepping procedure provided by TOUGH2 has therefore been modified to achieve better results in this respect.
- **Input routines.** Input routines have been implemented so that all dilation parameters can be defined using external files.

2.2 Further investigations on time-dependent dilation effects

In the main model, a local equilibrium between gas pressure and porosity is assumed for the dilation process. Equilibrium is supposed to establish instantaneously which means that no time-dependent effects are considered. This should be an acceptable approximation at least for slow transport processes.

On shorter time scales, time-dependent effects may come into play. This is especially important for the processes at the dilation front where high dilation rates can be found. Time-dependent effects may decide whether the propagation of the dilation zone and of the gas phase contained herein is dominated by the behaviour of the dilation front (i.e. by the border of the dilation zone) or by the permeability within the dilated zone (i.e. by the entire dilation zone): In the case of instantaneous equilibration, i.e. with no time-dependency, gas flow will

mainly be controlled by the gas permeability inside the dilated zone and to a much lesser extent by the propagation speed of the dilation front, which is fast due to the quick equilibration. The opposite is the case if the front propagation is delayed by a time-dependent dilation process. The permeability within the dilation zone then loses much of its importance.

In rock salt, a pressure-dependent velocity of the dilation front has been observed in laboratory and in-situ experiments if gas pressure is applied quickly (from the long-term perspective) /GRS 08/. Within the framework of this study it was therefore attempted to implement this time-dependent process as an alternative model into the TOUGH2 code. However, first test simulations showed a marked grid-dependency of the numerical solution if constant pressures were assumed at the dilation front (the assumption of constant pressures is a reasonable approximation in case of a slow front propagation). The reason for the observed grid dependency is probably the fact that the direction of gas flow at the dilation front can not be derived from pressure gradients but has to refer to the local orientation of the dilation front (the propagation direction should be orientated normal to the front). The latter, however, is dependent on the observation scale and was, on the element-scale, influenced by the rectangular structure of the grid that was used.

Several factors might be capable of mitigating the observed grid-dependency. If the propagation of the dilation front is fast enough to allow moderate pressure gradients to establish within the dilation zone, the dilation front will probably rather follow isobars than local grid structures. Grid-dependency might also be mitigated if the evolution of the stress field is simulated, too. The dilation front might then be inclined to follow planes of equal minimal principal stress. However, considering mechanical processes at the dilation front lies beyond the scope of the work planned for PAMINA work package 3.2. Since no satisfying results had been achieved, the alternative model with a pressure-dependent velocity of the dilation front is not presented in this report. Nevertheless, simulating this process may turn out to be important in the future.

3 Model description

The governing equations of TOUGH2 and EOS7 will be delineated according to /PRU 99/. Heat transport will not be considered which means that no energy balance equations will be presented in the following although they can be solved by TOUGH2. It also means that all processes are assumed to be approximately isothermal.

3.1 Conventional two-phase flow

Three components, water, brine and air, are considered by the equation-of-state module EOS7. Using a component index k (=1 for water, =2 for brine, =3 for the gas component), the following mass balance equations are solved by TOUGH2

$$\frac{\partial M^{\kappa}}{\partial t} = -\operatorname{div}\left(F^{\kappa}_{\mathrm{adv}} + F^{\kappa}_{\mathrm{dif}}\right) + q^{\kappa} \qquad (1)$$

where M^{κ} are local mass densities. $F^{\kappa}_{\mathrm{adv}}$ and $F^{\kappa}_{\mathrm{diff}}$ are advective and diffusive flow densities, respectively, and q^{κ} are source terms for each component. Note that hydrodynamic dispersion is not part of the standard TOUGH2 code.

Diffusive flow density of component k in phase β (β =1: gas phase, β =2: liquid phase) is given by

$$F^{\kappa}_{\beta} = -\phi\tau_0 \sum_{\beta} \tau_{\beta}(S_{\beta})\rho_{\beta} d^{\kappa}_{\beta} \nabla X^{\kappa}_{\beta} \qquad (2)$$

where ϕ denotes porosity, ρ_{β} the density of phase β, X_{β}^{k} the mass fraction and d_{β}^{k} the molecular diffusion coefficient of component κ in phase β. $\tau_0\tau_{\beta}(S_{\beta})$ is the tortuosity, which itself is split up into a rock dependent factor τ_0 and a saturation dependent factor $\tau_{\beta}(S_{\beta})$. Using effective diffusion coefficients equation (2) can be rewritten as

$$F^{\kappa}_{\beta} = -\sum_{\beta} D^{\kappa}_{\mathrm{eff},\beta} \nabla(\rho_{\beta} X^{\kappa}_{\beta}) \qquad (3)$$

with effective diffusion coefficient

$$D^{\kappa}_{\mathrm{eff},\beta} = \phi\tau_0\tau_{\beta}(S_{\beta}) d^{\kappa}_{\beta}. \qquad (4)$$

This equation will be needed later on to determine $d^{\mathrm{H2}}_{\mathrm{liq}}$ from effective diffusion coefficients.

The diffusion coefficients of gases is a function of pressure and temperature

$$d_\beta^\kappa(p,T) = d_\beta^\kappa(p_0,T_0)\frac{p_0}{p}\left(\frac{T+273.15\,°C}{273.15\,°C}\right)^\theta \tag{5}$$

with θ=1.80.

TOUGH2 offers three tortuosity models

$$\tau_0\tau_\beta = \tau_0 k_{r,\beta}(S_\beta) \quad \text{(relative permeability model)} \tag{6}$$

$$\tau_0\tau_\beta = \phi^{1/3} S_\beta^{\,10/3} \quad \text{(Millington-Quirk-Model)} \tag{7}$$

$$\tau_0\tau_\beta = \tau_0 S_\beta \quad \text{(constant diffusivity)} \tag{8}$$

of which the Millington-Quirk-Model will be applied. Assuming this model and using equations (4) and (5), the diffusion coefficient d_{liq}^{H2} at reference state (p_0, T_0) can be determined from the effective gas diffusion coefficient under full saturation $D_{eff,liq}^{air}$ by

$$d_{liq}^{air}(p_0,T_0) = \frac{D_{eff,liq}^{air}}{\phi^{4/3}}\frac{p}{p_0}\left(\frac{273.15\,°C}{T+273.15\,°C}\right)^\theta \tag{9}$$

where p and T specify the pressure and temperature applied in the diffusion experiment.

The advective flow density of a component in the mass balance equation (1) is defined by the flow densities F_β in the respective phases:

$$F_{adv}^\kappa = \sum_\beta X_\beta^\kappa F_\beta\,, \tag{10}$$

where X_β^κ is the mass fraction of component κ in phase β. The phase flows F_β in equation (10) are determined by a generalised Darcy law

$$F_\beta = -k_\beta \frac{k_{r,\beta}\rho_\beta}{\mu_\beta}(\nabla p_\beta - \rho_\beta g)\,. \tag{11}$$

Here, for phase β, k_β is the absolute and $k_{r,\beta}$ the relative permeability, ρ_β the density and μ_β the dynamic viscosity. g is the vector of gravitational acceleration. In the language of TOUGH2 the term

$$k_\beta \frac{k_{r,\beta}}{\mu_\beta}$$

is called “mobility”.

As a default, absolute gas permeability in equation (11) is set equal to the absolute liquid permeability, but TOUGH2 can account for a lowering of the absolute gas permeability at low pressures p by means of the Klinkenberg relation with Klinkenberg parameter b /KLI 41/

$$k_{gas} = k_{liq}\left(1+\frac{b}{p}\right). \tag{12}$$

Phase pressure p_β in the definition of the phase flows (11) is the sum of the gas pressure p_{gas} and the (negative) capillary pressure $p_{c,\beta}$ of phase β:

$$p_\beta = p_{gas} + p_{c,\beta}. \tag{13}$$

There are several options in TOUGH2 to define capillary pressure functions $p_{c,\beta}(S)$. Most simulations presented here will make usage of the van Genuchten function /GEN 80, PRU 99/

$$p_{c,liq} = -p_{entry}\left(S_{eff}^{\ -\lambda^{-1}} - 1\right)^{1-\lambda} \tag{14}$$

where p_{entry} is the apparent gas entry pressure and S_{eff} the effective saturation

$$S_{eff} = \frac{S_l - S_{lr}}{S_{ls} - S_{lr}} \tag{15}$$

with liquid saturation S_l, residual liquid saturation S_{lr} and maximum liquid saturation S_{ls}. Negative capillary pressure is held constant below a certain pressure limit $p_{c,min}$.

For equation (11) TOUGH2 offers several relative permeability functions. In the simulations presented here, relative permeability of the pore space unaffected by pathway dilation will be modelled using Corey’s curves /COR 54, PRU 99/

$$k_{r,liq} = S_{eff}^4 \tag{16}$$

$$k_{r,gas} = \left(1-S_{eff}\right)^2\left(1-S_{eff}^2\right) \tag{17}$$

with effective saturation

$$S_{\text{eff}} = \frac{S_{\text{l}} - S_{\text{lr}}}{1 - S_{\text{lr}} - S_{\text{gr}}}. \qquad (18)$$

Here, S_{l} is the liquid saturation, S_{lr} the residual liquid saturation, and S_{gr} the residual gas saturation, with $S_{\text{lr}} + S_{\text{gr}} < 1$.

3.2 Thermodynamic processes

Thermodynamic processes will be modelled using a modified version of the equation-of-state module EOS7, which in its original version considers two phases (gas phase and liquid phase) and three components (water, brine and air). For the application to a HLW repository with dominant production of H_2 it was necessary to change the gas component from air to H_2. This includes a redefinition of the molar mass, the specific enthalpy, the viscosity of the gas-vapour mixture and the Henry-Isotherm. Redefining the viscosity was important with regard to the conceptual model for the gas flow due to pathway dilation (see next chapter) since in this model the gas phase does not need to displace water in order to migrate, and this implies that the physical properties of the gas phase become very important for its flow. Using EOS7 instead of EOS5 makes it possible to consider saline groundwater or the transport of a tracer by using the brine component. However, no brine will be addressed in the simulations presented in this report. This simplifies the description of the thermodynamic model to the case of pure water in the following.

H_2 is assumed to behave like an ideal gas and gas pressure p_{gas} is assumed to be the sum

$$p_{\text{gas}} = p_{\text{H2}} + p_{\text{vapour}} \qquad (19)$$

of partial H_2 and vapour pressures p_{H2} and p_{vapour}, respectively. EOS7 does not account for any vapour lowering effects owing to capillary and phase adsorption effects. For this reason, vapour partial pressure p_{vapour} is set equal to the saturated vapour pressure. The latter is calculated by means of steam table equations given by the International Formulation Committee /IFC 67/.

H_2 partial pressure in (19) is calculated according to Henry's law

$$p_{\text{air}} = K_{\text{h}} x_{\text{liq}}^{\text{H2}}, \qquad (20)$$

where K_{h} is the inverse of Henry's constant and $x_{\text{liq}}^{\text{H2}}$ is the mol fraction of H_2 in the liquid phase. In EOS5, the coefficient K_{h} is set to

$$K_h = \max\left(1.379 \cdot 10^{-10}\,\text{Pa},\quad 1.697 \cdot 10^{-10}\,\text{Pa} - 1.272 \cdot 10^{-12}\,\text{PaK}^{-1} \cdot T\right)$$

which has been transferred to the EOS7 module. The mol fraction $x_{\text{liq}}^{\text{H2}}$ in equation (20) is calculated from the mass fractions $X_{\text{liq}}^{\text{H2}}$ and $X_{\text{liq}}^{\text{water}}$ of H_2 and water in the liquid phase, respectively, by

$$x_{\text{liq}}^{\text{air}} = \frac{X_{\text{liq}}^{\text{air}} \mu_{\text{air}}^{-1}}{X_{\text{liq}}^{\text{air}} \mu_{\text{air}}^{-1} + X_{\text{liq}}^{\text{water}} \mu_{\text{water}}^{-1}}, \tag{21}$$

where μ_{H2} is the molar mass of H_2 and μ_{water} is the molar mass of water. Liquid water density and vapour density are calculated using the steam table equations mentioned above.

A new viscosity function for H_2-vapour mixtures was introduced by GRS according to kinetic gas theory with data from /LAN 69/ and some pressure correction derived from the viscosity data used in the EOS5-module. Pressure has only minor effect on viscosity.

3.3 Gas flow due to pathway dilation

3.3.1 Conceptual model

Due to the dependency of the capillary forces on the pore size, it is assumed that a gas phase will first enter the largest pores of a saturated clay and thus it is assumed that dilation will first affect these large pores. Postulating that dilation tends to locate at pores which are already dilated, only a small pore fraction will be subjected to pathway dilation. Dilating pores are partially filled with water. However, this water, which only presents a very small amount of the water content of the clay, is supposed to be irrelevant in terms of liquid phase and gas phase flow and in terms of capillary pressure for the following reasons:

- The main water content of the clay will only be able to flow inside the non-deformed pore space due to the elevated gas pressure in dilated pores.
- It is assumed that the gas phase will be able to move by deforming the rock matrix without needing to displace pore water.
- If water filled pores are dilated by the gas phase, the capillary pressure will drop due to the increased pore radii. However, the amount of water within dilated pores is very small and can probably be displaced from these pores easily. As soon as this small quantity of water has been removed the dilated pores, capillary pressure will be controlled by the properties of the non-dilated pores. Dilation therefore should not have any major influence on capillary pressures within the assumptions mentioned above (if capillary pressure is expressed as a function of liquid content).

This means that the liquid phase will not take any major advantage from the dilated pores. Thus, a special feature of the proposed conceptual model is that dilation does not affect the flow of the liquid and gas phase equally.

The original porosity in the non-dilated state will be called *primary porosity* in the following, whereas the porosity gained by dilation will be called *secondary porosity*. It has to be noted that dilated pores contribute to both, primary and secondary porosity. However, the pore fraction that belongs to the primary porosity is supposed to be of minor relevance for the flow processes for the mentioned reasons.

In the framework of the PAMINA project, it is assumed that there is no significant hydro-mechanical interaction between dilated and non-dilated pores. However, hydro-mechanical coupling may be introduced into the code in the future.

The consequence of all these assumptions is that water will be present only in the primary porosity and will not notice any dilation effects. Capillary pressures thus remain constant in relation to the water content and water flow will be enhanced only by the pressure of the intruding gas phase but not by dilation of water filled pores. Experimental data indeed indicate that the amount of water displaced by creation of additional gas pathways is very small for both, bentonite /HOC 04/ and natural clays /ROD 03/. In the model presented here, the gas phase is expected to be able to flow through the clay without needing to displace water, i.e. it will be able to move even if the pore water is completely immobile (which might e.g. be forced by boundary conditions or by very rigorous gas entry pressures).

It is assumed that dilation processes are fast in relation to the pressure build up (quick equilibration of pressure and porosity) and that there aren't any memory effects. It shall be possible to describe flows at element scale by Darcy's law (no intermittent gas flow), which implies that a homogeneous representation of dilation effects must be possible. It is assumed that the hydraulic effects of pathway dilation can be described adequately by a pressure-dependent porosity and a pressure-dependent anisotropic gas permeability.

The assumed quick equilibration implies that the propagation of the front of the dilation zone does not show any kinetic effects and does not give any resistance to the flow of the gas phase. This means that the dilation front can propagate easily through the rock as long as there is sufficient gas supply.

3.3.2 Physical and mathematical model

A pressure-dependent porosity has been introduced into the code TOUGH2/EOS7 in order to create additional storage capacity for the gas phase that allows the gas phase to flow without needing to displace water. The increase of porosity was modelled independently from the porosity-change-feature of TOUGH2 (invoked by prescribing a pore compressibility or expansivity) which just affects the fluxes but not the pore volume. Since porosity changes affect the local physical state (in terms of liquid saturation, capillary pressure, pressure and

density of the liquid and gas phase, pressure and density of gas phase, water density, vapour density, density of dissolved H_2, and internal energy), state changes due to the expansion or compression of the pore space were calculated along the thermodynamic processes implemented in the used EOS7-module. Thus, the pressure-dependent change of porosity of TOUGH2-PD does not only alter hydraulic properties but also considers the thermodynamic processes triggered by pore expansion or compression.

An anisotropy of gas flow due to dilation is likely with regard to the textural anisotropy of clay stone. However, the sources of anisotropy is not easy to identify. Anisotropy might e.g. be caused by an anisotropic stress field or rock fabric which favours the growth, opening and interconnection of more or less planar pores with specific orientation and shape. Another reason for anisotropy might be that dilation thresholds vary with the orientation of planar pores due to an anisotropic stress state. It is not clear whether tensile strength, which is different normal and parallel to the bedding plane, significantly influences dilation thresholds if gas pressure increases very slowly. Marschall et al. (/MAR 05/) assume that clay-rich rock cannot withstand long-term gas pressures with a magnitude greater than the minimum principal stress acting on the rock mass. Thus, the mechanical processes causing an anisotropy of gas flow are complicated and hard to predict without further experimental substantiation and hydro-mechanically coupled simulations. For this reason, a simple anisotropy model was introduced into TOUGH2 by giving the user of the code the opportunity to define a set of micro-crack networks, each with its own dilation threshold, anisotropic permeability-pressure relationship, and porosity-pressure relationship.

Equation (11), which TOUGH2 uses for the calculation of the gas phase flow F_{gas}, was redefined by adding a term describing the sum of the gas phase fluxes in n micro-crack networks

$$F_{\mathrm{gas}} = -\left(\underbrace{\frac{\rho_{\mathrm{gas}}}{\mu_{\mathrm{gas}}} k \; k_{\mathrm{r,gas}} \mathbf{I}}_{\substack{\text{determines the gas flux} \\ \text{in the primary porosity}}} + \underbrace{\frac{\rho_{\mathrm{gas}}}{\mu_{\mathrm{gas}}} \sum_{i=1}^{n} \mathbf{K}_{\mathrm{dil},i} k_{\mathrm{dil},i}(p_{\mathrm{gas}})}_{\substack{\text{determines the gas flux in the secondary} \\ \text{porosity of } n \text{ micro-crack networks}}} \right) (\nabla p_{\mathrm{gas}} - \rho_{\mathrm{gas}} g) \; , \qquad (22)$$

where k is the absolute and $k_{\mathrm{r,gas}}$ the relative gas permeability, ρ_{gas} the density, μ_{gas} the dynamic viscosity of the gas phase, and g the vector of gravitational acceleration. $k_{\mathrm{dil},i}$ is the pressure-dependent gas permeability of micro-crack network i and tensor $\mathbf{K}_{\mathrm{dil},i}$ is introduced in order to make gas permeability dependent on flow direction.

There are several possibilities to introduce a pressure-dependency of the gas flux e.g. by defining a pressure-dependent relative gas-permeability or intrinsic permeability. Modelling the gas flux through the primary and secondary porosity independently, as it was done here, implies that these fluxes are physically independent which is in accordance with the conceptual model. This approach also allows a decoupling of weighting schemes for the flow

in dilated and non-dilated pores. By defining an upwind weighting scheme for the gas flux in the secondary porosity the intended easy propagation of the dilation front according to the assumption of quick equilibration can be achieved.

For $k_{\mathrm{dil},\,i}$ a power law

$$k_{\mathrm{dil},\,i}(p_{\mathrm{g}}) \overset{\mathrm{def}}{=} \begin{cases} 0 & \text{for} \quad p_{\mathrm{g}} \le p_{\mathrm{thr},i} \\ \left(\dfrac{p_{\mathrm{g}} - p_{\mathrm{thr},i}}{\Delta p} \right)^{\alpha} \Delta k_{\mathrm{dil},\,i} & \text{for} \quad p_{\mathrm{g}} > p_{\mathrm{thr},i} \end{cases} \tag{23}$$

was used, where $\alpha > 1$ is an arbitrary exponent and Δp defines a pressure interval $[p_{\mathrm{thr},i},\, p_{\mathrm{thr},i} + \Delta p]$ over which gas permeability changes by $\Delta k_{\mathrm{dil},\,i}$.

The porosity ϕ is defined as the sum of the initial porosity ϕ_0 and the porosity of each micro-crack network ϕ_i:

$$\phi = \phi_0 + \sum_{i=1}^{n} \phi_i(p_{\mathrm{g}}) \,. \tag{24}$$

Assuming that micro-cracks are parallel plates which open according to a linear elastic law a linear relation between crack porosity ϕ_i and gas pressure

$$\phi_i(p_{\mathrm{g}}) \overset{\mathrm{def}}{=} \begin{cases} 0 & \text{for} \quad p_{\mathrm{g}} \le p_{\mathrm{thr},i} \\ \dfrac{p_{\mathrm{g}} - p_{\mathrm{thr},i}}{\Delta p} \Delta\phi & \text{for} \quad p_{\mathrm{g}} > p_{\mathrm{thr},i} \end{cases} \tag{25}$$

is postulated which shall be called *"dilation relationship"* in the following. As above, p_{g} is the gas pressure and p_{thr} a threshold pressure for the onset of dilation. Δp defines a pressure interval $[p_{\mathrm{thr},i},\, p_{\mathrm{thr},i} + \Delta p]$ over which porosity changes by $\Delta\phi$. Other, e.g. non-linear, dilation relationships may be defined by the user with the obligation that porosity has to increase monotonously with pressure.

3.3.3 Numerical implementation

3.3.3.1 Semi-explicit solution of flow equations

Due to the strong non-linearity of the relationships describing the dilation behaviour, porosity and permeability are changed after completion of a time step in order to avoid convergence problems. This implies that the flow equations are solved with constant porosities and permeabilities which belong to the previous time step. With regard to this, the flow equations are now solved semi-explicitly by TOUGH2.

3.3.3.2 Porosity change

To comply with the user-defined relationships between porosity and pressure and to guarantee mass conservation, porosities, pressures and saturations are changed after each time step. This is done by simulating isothermal compression or expansion of the pore space according to the thermodynamic processes implemented in the EOS7 module (see explanation below). Although TOUGH2 allows the definition of a pressure-dependent pore compressibility it was not possible to use this feature to simulate pore expansion and compression since TOUGH2's pore compressibility feature does not affect the physical porosity but only the calculation of mass flows by assuming that all mass concentrations are linearly increased by the given porosity increase. Yet, a physical increase of porosity is necessary in order to let a gas phase flow though a rock with immobile liquid phase. Therefore, a real porosity change was implemented into the code.

3.3.3.3 Equilibration

After the flow equations have been solved with constant porosities and permeabilities, local pressures and porosities usually do not satisfy the dilation relationship (25). Thus, after a time step, compression or expansion of the pore space has to take place by adapting the TOUGH2 primary variables in order to satisfy the dilation relationship. Since the user may define arbitrary dilation relationships (with the obligation that porosity increases monotonously with pressure) an iterative method is needed to equilibrate gas pressure and porosity. A slightly modified root-finding algorithm of /PRE 96/ is used to find a gas pressure change which would lead to a porosity–pressure pair that satisfies the dilation relationship (25) with sufficient accuracy. This is done for each grid element. The primary variables are updated in advance.

Calculating the porosity change from a given pressure change is not straightforward. Each porosity change in a grid element affects its hydraulic and thermodynamic state. In particular such changes influence liquid saturation, capillary pressure, the density of water, vapour and dissolved H_2, the pressure and density of the liquid and gas phase, and the internal energy. This implies that thermodynamic processes have to be considered in order to calculate the porosity change that belongs to a certain pressure change without violating mass conservation. For this purpose an "inverse" EOS routine has been derived from the standard

EOS7 routine in this study (temperatures are held constant). The inverse EOS routine has been implemented with high accuracy with regard to the conservation of the mass of the gas component and to the sum of the masses of water and brine (see test results in section 4.1). To avoid iterative determination of primary variables in the inverse EOS routine, the brine mass is calculated using the brine mass fraction before (not after) porosity change. This causes some minor errors in the water-brine mass ratio. However, for considerations of gas transport in deep geological repositories small errors in the mass conservation of the brine component should be of minor importance.

The component masses which have to be conserved cannot be derived directly from the primary variables with accuracy. The reason for this is that the primary variable 'gas saturation' has the meaning of a gas saturation *after* evaporation of water and dissolution of the gas component has taken place. Thus, thermodynamic processes have to be considered to calculate component masses from the primary variables (this is done by the EOS module) or, vice versa, to determine primary variables for given component masses.

3.3.3.4 Decoupling of flows

The weighting procedure for the gas permeability has been completely decoupled from TOUGH2's weighting procedure for the relative permeabilities and "mobilities" (*relative permeability* x *absolute permeability* / *viscosity*) of the undisturbed matrix. This means that both terms

$$\frac{\rho_\beta}{\mu_\beta} k_\beta k_{\mathrm{r},\beta} \mathbf{I} + \frac{\rho_\beta}{\mu_\beta} \sum_{i=1}^{n} \mathbf{K}_{\mathrm{dil},i} k_{\mathrm{dil},i}(p_\mathrm{g})$$

of equation (22) can be weighted independently. The weighting procedure for the first term can be controlled using the TOUGH2 input. Upstream weighting has been chosen for the second term to allow an easy propagation of the dilation front according to the assumptions made.

3.3.3.5 Time step control

The initial code tests (see section 4.2) showed that the automatic time step control provided by TOUGH2 is not sufficient to simulate the dilation-controlled transport process appropriately. Therefore, an additional criterion for the reduction of time step widths was introduced. A time step is now repeated with a reduced time step width if

$$\exists\, i: (p_t^i \geq p_{\mathrm{thr}}^i \;\wedge\; |p_t^i - p_{t+\Delta t}^i| > p_{\mathrm{limit}}) \vee (p_t^i < p_{\mathrm{thr}}^i \;\wedge\; p_{t+\Delta t}^i \geq p_{\mathrm{thr}}^i \;\wedge\; p_{t+\Delta t}^i - p_{\mathrm{thr}}^i > p_{\mathrm{limit}})$$

where p_t^i and $p_{t+\Delta t}^i$ is the pressure in element i before and after a time step, respectively, p_{thr}^i is the minimal dilation threshold at element i, and p_{limit} is the positive maximum pressure change per time step.

In order to avoid oscillations, p_{limit} should be chosen small enough to prevent the first dilation event in element i to cause a pressure drop below the dilation threshold $p_{\text{thr}}{}^{i}$. The proposed time step control also limits the amount by which the dilation relationship (25) is violated.

4 Model tests

Several tests have been conducted to investigate the dilation behaviour of a single element and of a column of elements. In order to concentrate on the effect of dilation, transport in the undisturbed matrix is inhibited by setting the absolute (i.e. intrinsic) permeability to zero in all test cases.

4.1 Behaviour of a single element

A geometric model consisting of two elements is considered. Figure 4-1 shows the geometry of the grid that has been used.

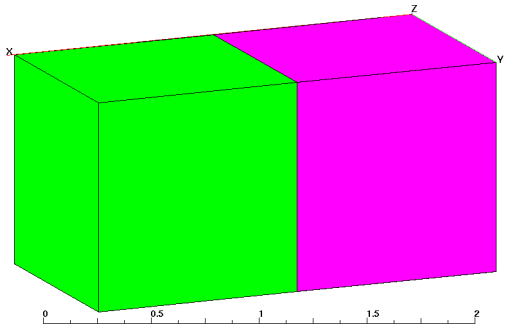

Figure 4-1: Grid used to evaluate the behaviour of a single element.

The grid has been build out of two elements, each with cubic geometry and a volume of 1 m³. The right element (“element 2”) does not change its state and serves as a fixed-pressure boundary for the left element (“element 1”) whose behaviour will be evaluated. Element 2 is completely filled with gas which is under a pressure of 11 MPa. These conditions remain unchanged during the simulation.

At time $t = 0$, element 1 is almost fully saturated with water (gas saturation S_g is set to 1E-10 – the rationale behind this is explained below) and under a pressure of 10 MPa. The pressure threshold for the onset of dilation is set to 10 MPa so that dilation starts immediately after the first flow of gas from element 2 to element 1. Gas flow through the matrix is inhibited by an intrinsic permeability of zero for both elements.

Initial porosity is set to 0.1 for both elements. For element 1, the following dilation relationship is defined:

$$\phi_{\mathrm{dil}}(p_{\mathrm{g}}) = \begin{cases} 0 & \text{for} \quad p_{\mathrm{g}} \le 10\,\mathrm{MPa} \\ \dfrac{p_{\mathrm{g}} - 10\,\mathrm{MPa}}{1\,\mathrm{MPa}} \cdot 0.0001 & \text{for} \quad p_{\mathrm{g}} > 10\,\mathrm{MPa} \end{cases}$$

According to this, porosity varies linearly from 0.1 to 0.1001 over the considered pressure interval of 1 MPa. Due to the upstream weighting of gas permeability, gas flows under a constant permeability of 1E-19 m², which is the permeability of element 2.

4.1.1 Initial gas saturation

Elements which do not contain any gas phase can not dilate because the implemented dilation procedure affords a gas phase that can be expanded. First test simulations have indicated that gas can flow even into fully saturated elements by compression of the liquid phase. This allows the formation of a gas phase, which can be expanded subsequently. However, if the inflow of gas is too small, the gas which flows into the saturated element will entirely be dissolved in the liquid phase without creating a gas phase that could be expanded. In this case, pressures rise above dilation thresholds but no dilation will take place. Consequently, porosity “explodes” as soon as a gas phase develops.

To allow dilation of elements which are fully saturated with an immobile liquid phase, one should therefore not rely on the compressibility of the liquid. Instead, a very small portion of gas should be added to every grid element, in order to enable the dilation mechanism. This strategy also avoids some numerical problems of TOUGH2 connected to the appearance and disappearance of a phase.

Figure 4-2 displays the pressure evolution in element 1 for different small initial gas saturations. No significant difference can be noticed between initial gas saturations of 1E-10 and 1E-4 (the latter is equal to the maximal porosity increase due to dilation). This shows that the model is quite insensitive to the magnitude of the initial gas saturation and works fine even with very small initial gas saturations.

In Figure 4-2, a different behaviour can be noticed if the initial saturation is as large as 0.1. In this case, the dilation mechanism is not able to decrease gas pressures because the maximal porosity created by dilation (0.0001) is too small compared to the porosity filled by the gas phase (0.1). One should therefore take care that the initial gas saturation of an element which is thought to be fully saturated with water stays well below the maximum porosity increase that can be achieved by dilation.

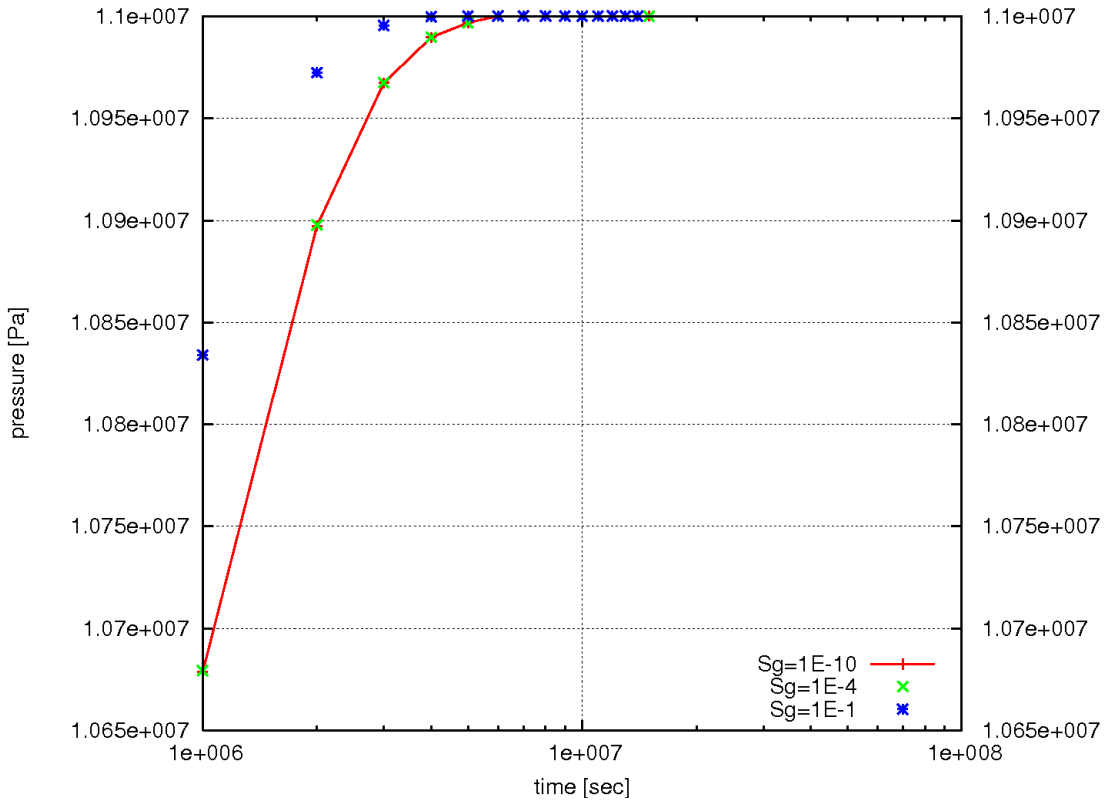

Figure 4-2: Pressure evolution in element 1 with different initial gas saturations (Sg). Time step width is 1E+6 seconds.

4.1.2 Equilibration and mass conservation

Five simulations with different time steps widths of 1, 100, 1E+4, 1E+6, and 1E+8 seconds have been performed to investigate the accuracy of equilibration and the conservation of component masses.

As mentioned above, flow equations are solved by TOUGH2 with the assumption of constant porosities. Consequently, porosities and pressures usually do not satisfy the dilation relationship (25) after the flow equations have been solved. This fact is illustrated by Figure 4-3, which shows the porosity and pressure evolution in element 1 after the flow equations have been solved and before the dilation procedure has been invoked. Especially for time step widths larger than 1E+04 seconds, porosity-pressure pairs are located on the right side of the dilation relationship $\phi(p)$ indicating an overshoot of pressures due to the absence of dilation during the flow process. Pressure overshoot is largest for small total porosities because small gas injections can create large pressure increases if gas saturation is small. Simulations with time step widths of 1 and 100 seconds do not show any significant deviations from the dilation relationship, even for small porosities.

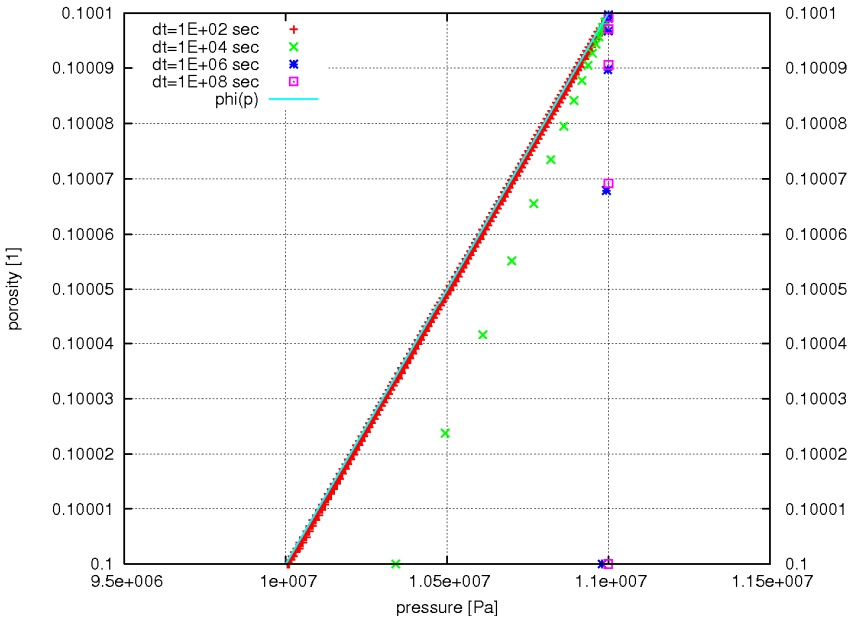

Figure 4-3: Porosity-pressure state in element 1 for different time steps widths dt before dilation has taken place. “phi(p)” is the given dilation relationship.

Figure 4-4 shows the porosity and pressure evolution of element 1 *after* the dilation procedure has been invoked. Apparently, the code equilibrates correctly with regard to the dilation relationship (25).

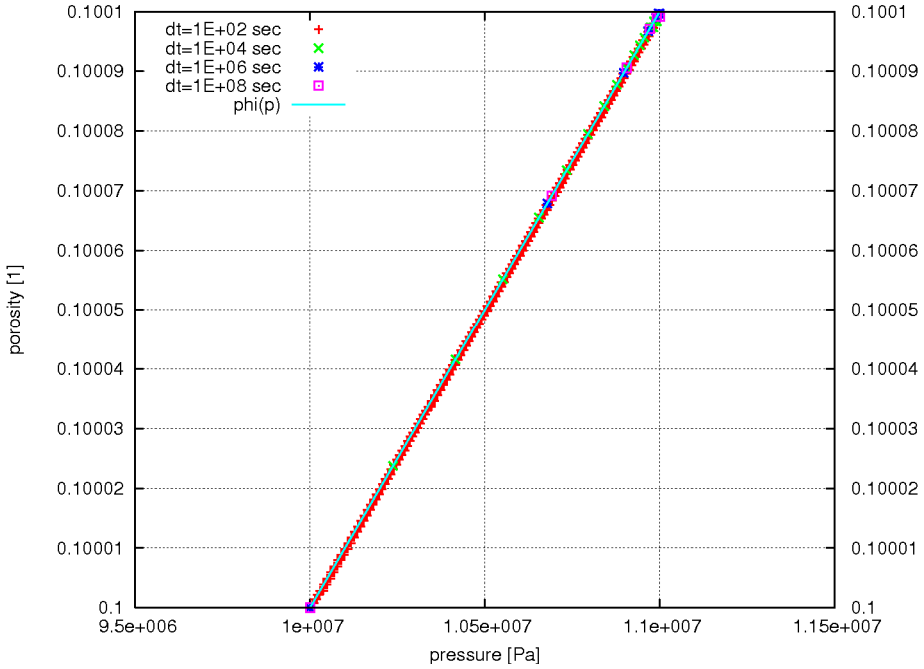

Figure 4-4: Porosity-pressure state in element 1 for different time steps widths dt after dilation has taken place. “phi(p)” is the given dilation relationship.

To investigate, whether component masses are conserved correctly during the dilation procedure, component masses before and after porosity change and adaptation of primary variables have been compared. Relative errors of less than 1E-15 with regard to the mass of water and relative errors of less than 1E-13 with regard to the mass of H_2 were measured for all simulations, demonstrating the high precision of the implemented “inverse EOS module”, which is needed to calculate primary variables for given component masses.

4.1.3 Response time

Since porosities are kept constant during the flow process, pressure increase in element 1 is overestimated and gas flow is underestimated every time step. Consequently, the pressure evolution in element 1 will suffer a delay which is dependent on the time step width.

Figure 4-5 displays the pressure evolution of element 1 for time steps widths of 1, 100, 1E+4, 1E+6, and 1E+8 seconds. For small time step widths of 1 and 100 seconds, pressure curves are almost identical. Figure 4-3 had indicated the absence of pressure overshooting for these time widths, showing that these simulations are very close to what would be expected if the flow equations had been solved implicitly with pressure-dependent porosity and permeability.

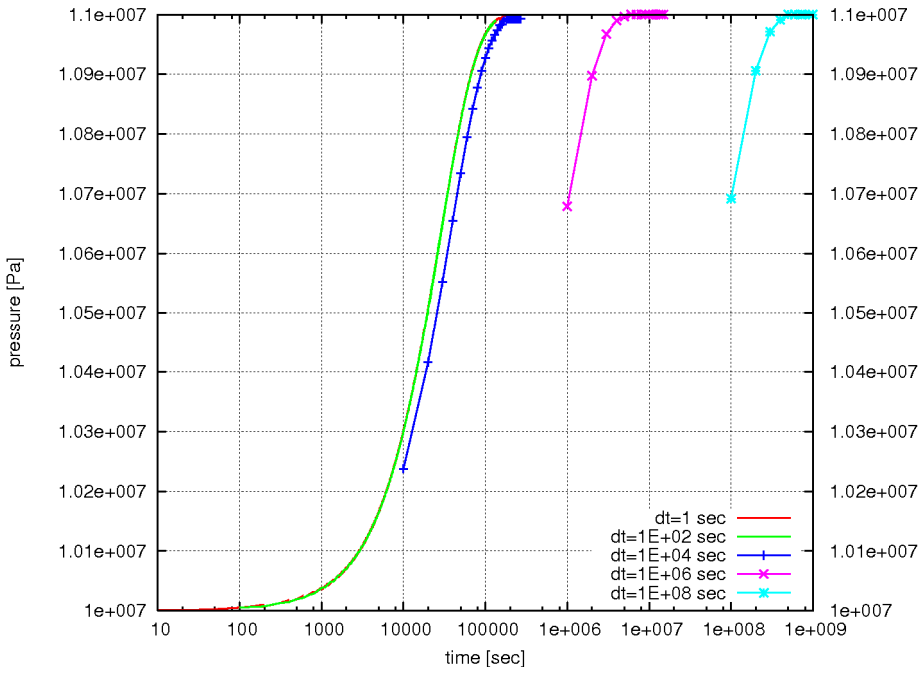

Figure 4-5: Pressure evolution in element 1 for different time step widths Δt (“dt”).

Looking at the time t_{90} at which the pressure curve passes the 90%-value of the maximum pressure change (1 MPa), the delay of the pressure signal produced by time step widths larger than 1 second compared to a time step width of 1 second can be estimated by $t_{90}(\Delta t)$ - $t_{90}(1\ \text{sec})$.

Doing this, a power law relationship can be noticed between time step width and the delay time (Figure 4-6). Delay time and the time step width are in the same order of magnitude.

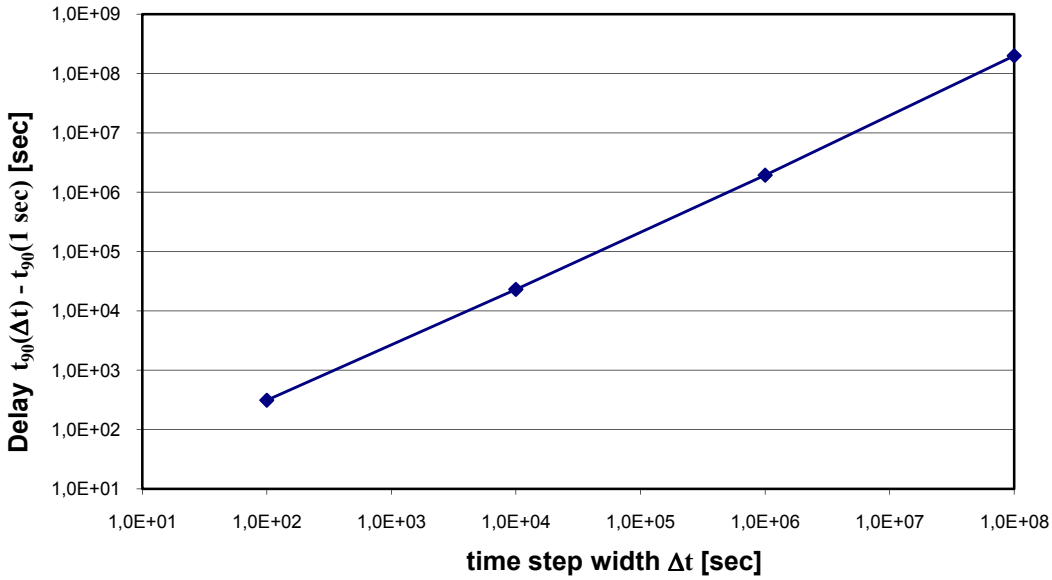

Figure 4-6: Delay of the transgression of the 90%-value of the total pressure increase in element 1.

4.2 Transport in a column

A 1-dimensional model will be used to investigate the transport of a gas phase by a propagating dilation zone. Figure 4-7 displays the considered grid geometry. A horizontal column with a length of 1.01 m and a square section of 0.01 m² is considered. The first element has a length of 1 cm and contains a gas source. The remaining 1 m of the column is divided into *n*=10, 100 or 1000 elements depending on the test case.

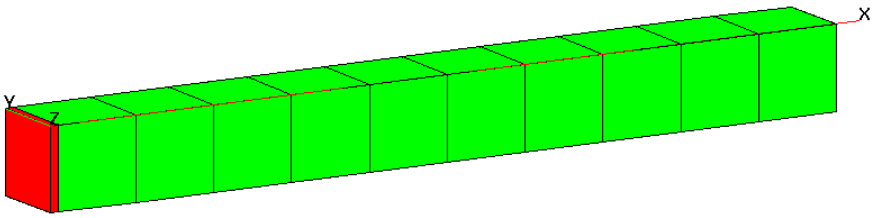

Figure 4-7: Grid for 1-dimensional considerations (x-direction is considered as “length” of the column). The red element on the left side holds the gas source.

Intrinsic permeability is set to zero and the initial porosity to 0.1 for the entire domain. Initial gas saturation is 1E-10 in all elements except for the first element, where gas saturation is set to 0.0001 in order to facilitate gas injection.

All elements are allowed to dilate (also the source element) and the effects of dilation are described by

$$\phi_{\mathrm{dil}}(p_{\mathrm{g}}) = \begin{cases} 0 & \text{for} \quad p_{\mathrm{g}} \le 10\,\mathrm{MPa} \\ \dfrac{p_{\mathrm{g}} - 10\,\mathrm{MPa}}{1\,\mathrm{MPa}} \cdot 0.0001 & \text{for} \quad p_{\mathrm{g}} > 10\,\mathrm{MPa} \end{cases}$$

$$k_{\mathrm{dil}}(p_{\mathrm{g}}) = \begin{cases} 0 & \text{for} \quad p_{\mathrm{g}} \le 10\,\mathrm{MPa} \\ \dfrac{p_{\mathrm{g}} - 10\,\mathrm{MPa}}{1\,\mathrm{MPa}} \cdot 10^{-19}\,\mathrm{m}^2 & \text{for} \quad p_{\mathrm{g}} > 10\,\mathrm{MPa} \end{cases}$$

Initial pressure is 9.99 MPa for all elements. This is very close to the dilation threshold pressure. H_2 is injected into the first element at a rate of 1E-8 kg/s.

4.2.1 Grid-dependency

To investigate the grid-dependency of the dilation-controlled transport, the main part of the column (the last metre) is divided into 10, 100, and 1000 elements. The initial time step width is set to 1 second and automatic time stepping is enabled with an upper step width limitation of 50 seconds.

Figure 4-8 shows the pressure distribution 4000 seconds after the beginning of gas injection. The most important difference between the different grid resolutions is visible at the front of the dilated zone. The dilation front is very sharp for a resolution of 1000 elements per metre and blurs with decreasing resolution. It stands to reason that a lower grid resolution increases numerical dispersion, which leads to a faster propagation of the dilation front. Gas pressures at the source therefore decrease slightly with decreasing resolution (see also Figure 4-9). Except for this phenomenon, the dilation-controlled transport does not exhibit any obvious grid-dependency.

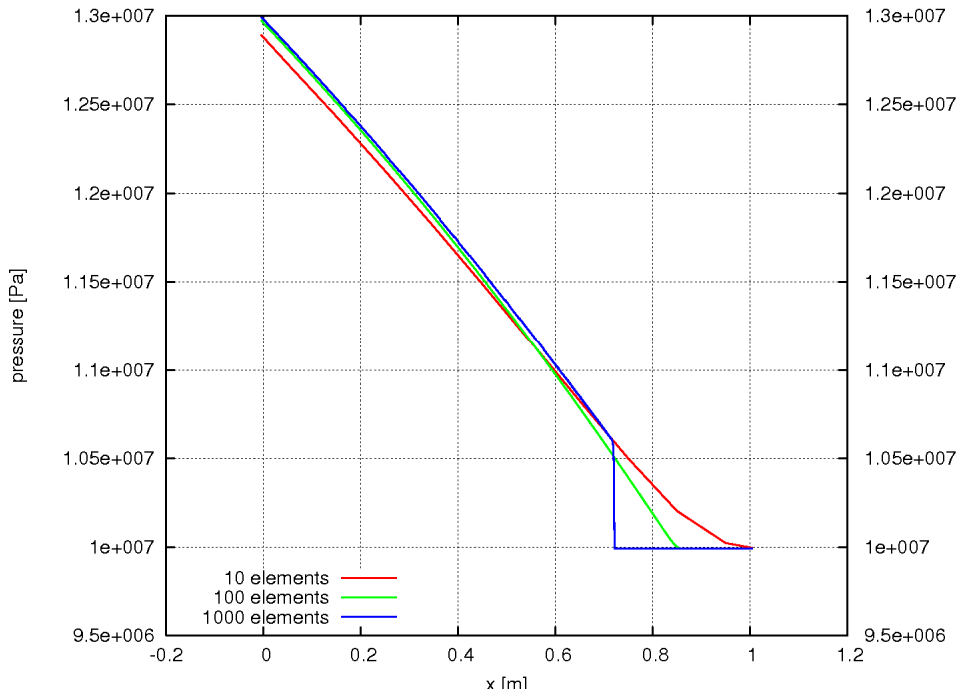

Figure 4-8: Pressure distribution along the column after 4000 seconds for different grid resolutions.

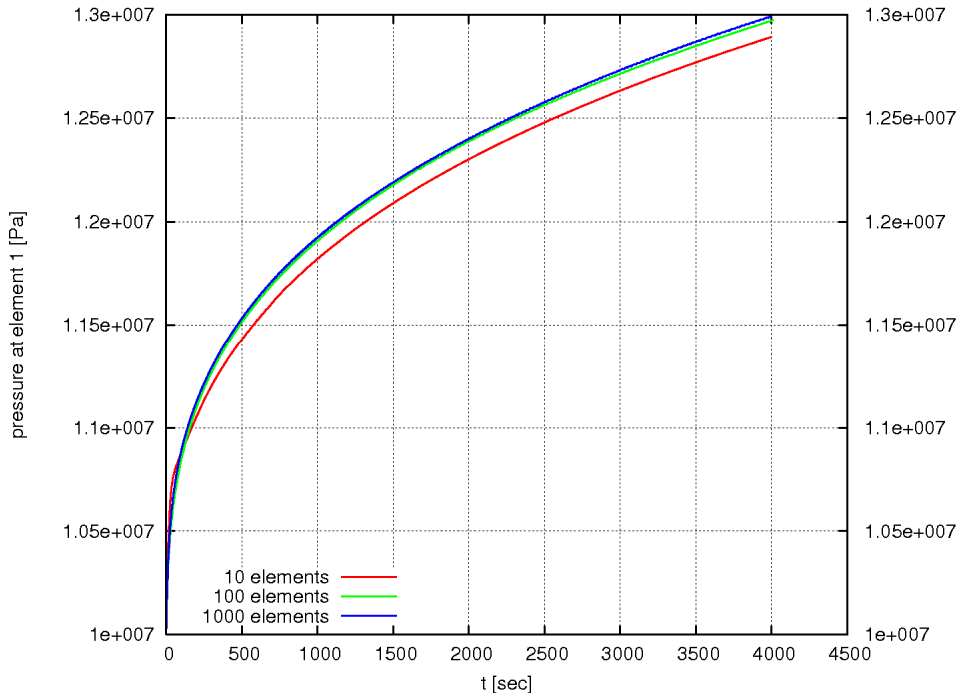

Figure 4-9: Pressure evolution at the source element for different grid resolutions.

4.2.2 *Time step width*

If gas is injected into a medium which is fully saturated with water, special attention has to be paid to the maximum time step width. Figure 4-10 again shows the pressure evolution at the source element for different time step widths of Δt=1, 10, and 100 seconds. There is a distinct overshoot of gas pressure if the time step width is as large as 100 seconds. Figure 4-11 displays that the dilation front has not propagated as far as with time step widths of 1 or 10 seconds.

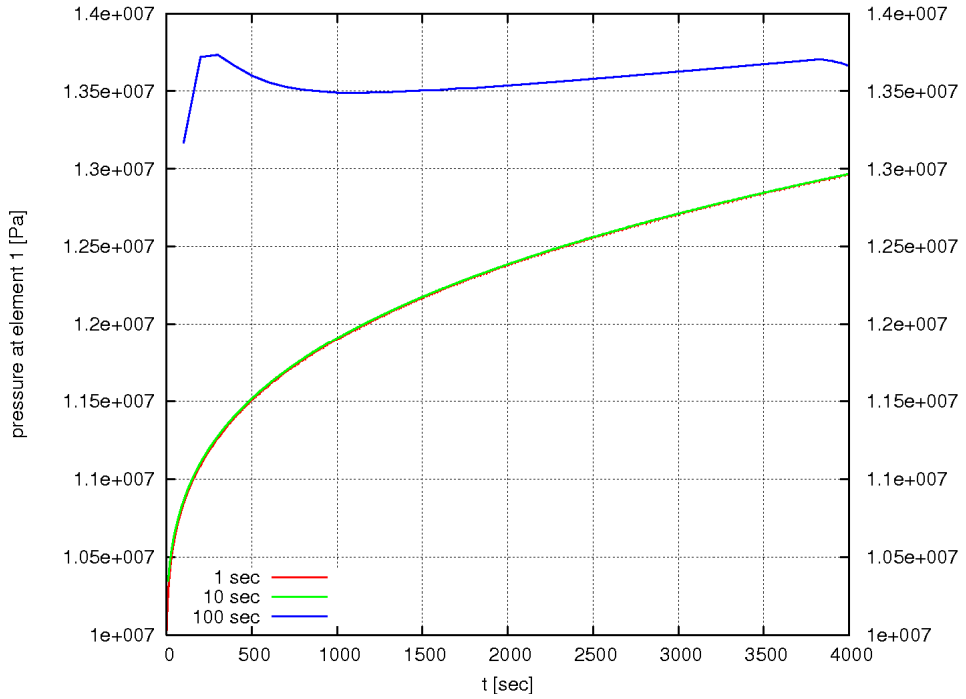

Figure 4-10: Pressure evolution at the source element for different time step widths.

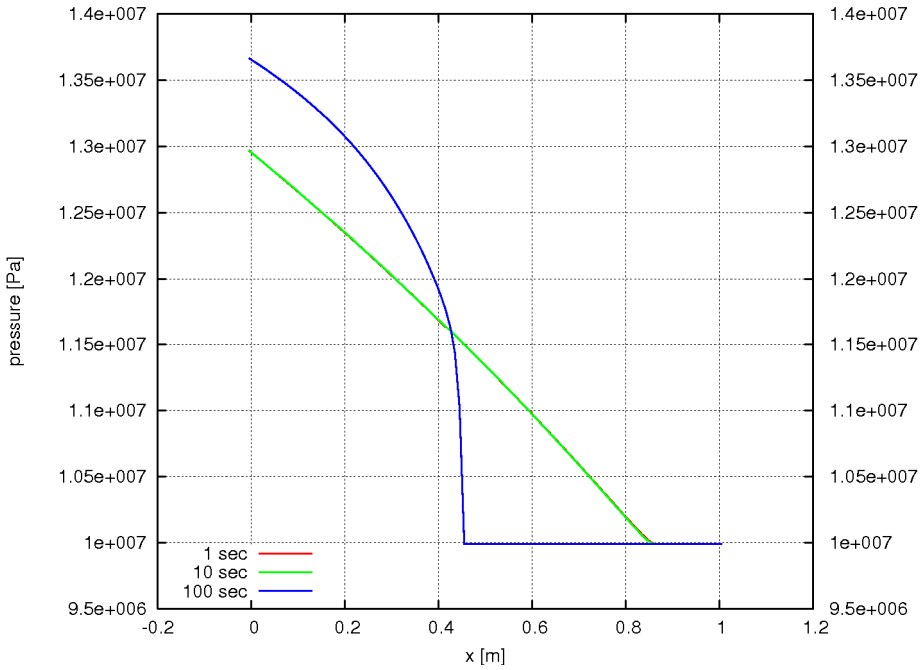

Figure 4-11: Pressure distribution along the column after 4000 seconds for different time step widths.

Obviously, for Δt=100 seconds, the gas phase does not manage to escape fast enough from the source, which forces the gas pressure to rise in the source element. The reason for this insufficient transport is probably the observed delay of the dilation process, which is more intense with increasing time step width (see Figure 4-6).

It was investigated whether this effect is also encountered if TOUGH2's automatic time step control is enabled. The red curve in Figure 4-12 shows the pressure evolution in the source element with TOUGH2's automatic time step control. The simulation was initiated with a very long time step width which was then reduced by TOUGH2 in order to perform the first time step. The curve shows the same pressure overshoot that was noticed before and this indicates that the automatic time step control provided by TOUGH2 is not sufficient to simulate the dilation-controlled transport process appropriately.

A simple solution for this is to reduce the time step width by limiting the maximal absolute pressure change |Dp| that is allowed to occur in dilated elements or in elements which will be dilated after the time step. A time step is repeated with a reduced time step with if

$$\exists\, i{:}\,(\, p_t^{\,i} \geq p_{\mathrm{thr}}^{\,i} \;\wedge\; |\, p_t^{\,i} - p_{t+\Delta t}^{\,i}| > p_{\mathrm{limit}}\,) \;\vee\; (p_t^{\,i} < p_{\mathrm{thr}}^{\,i} \;\wedge\; p_{t+\Delta t}^{\,i} \geq p_{\mathrm{thr}}^{\,i} \;\wedge\; p_{t+\Delta t}^{\,i} - p_{\mathrm{thr}}^{\,i} > p_{\mathrm{limit}})$$

where $p_t^{\,i}$ and $p_{t+\Delta t}^{\,i}$ is the pressure in element i before and after a time step, respectively, $p_{\mathrm{thr}}^{\,i}$ is the minimal dilation threshold at element i, and p_{limit} is the positive maximum pressure change per time step.

In order to avoid oscillations, p_{limit} should be chosen small enough to prevent the first dilation event in element i to cause a pressure drop below the dilation threshold $p_{\text{thr}}{}^{i}$. The proposed time step control also limits the amount by which the dilation relationship (25) is violated. In the test case, good results were achieved if pressure changes per time step were equal or smaller than 1 MPa (see Figure 4-12).

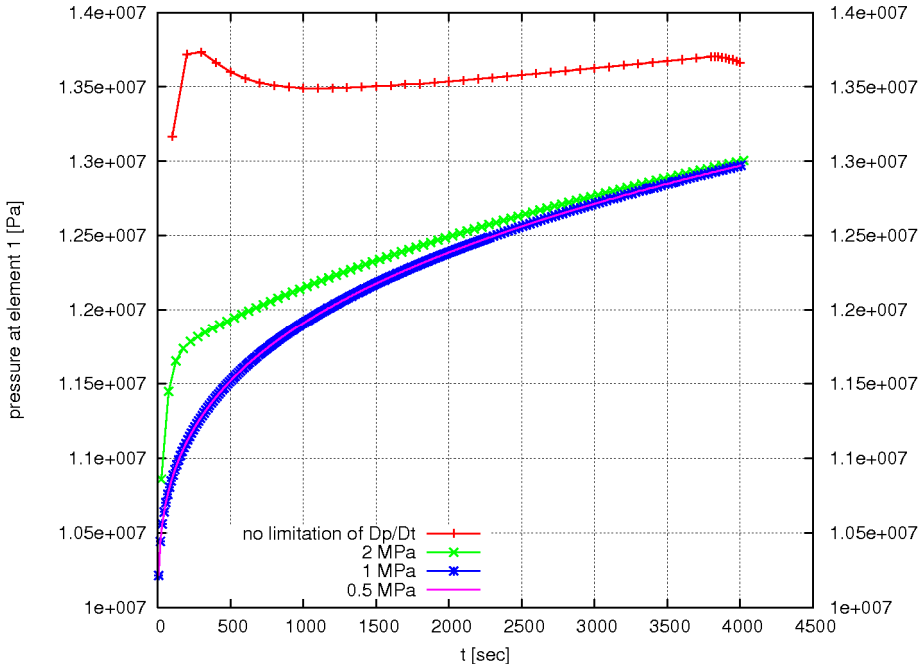

Figure 4-12: Pressure evolution at the source element for different time stepping procedures. The red curve refers to the standard procedure of TOUGH2. The other curves were achieved by limiting the maximal absolute pressure change per time step to 2 MPa, 1 MPa, and 0.5 MPa.

4.3 Summary of findings

The code TOUGH2 has been successfully extended to simulate pressure-dependent porosities and gas permeabilities due to the process of pathway dilation. Anisotropy of dilation-controlled gas transport can be expressed by defining sets of micro-crack systems with anisotropic characteristics. Dilation commences when gas pressures exceed certain pressure thresholds which are defined relative to the minimal principal stresses and independently for the different micro-crack systems. The automatic time stepping routine of TOUGH2 has been modified in order to limit numerical errors arising from the semi-explicit formulation of dilation-controlled gas transport.

The standard gas component of the EOS7 module has been changed from air to H_2 by changing the molar mass, the specific enthalpy, the Henry-Isotherm, and the viscosity of the gas-vapour mixture. Since there is no EOS module which defines viscosity for H_2-vapour

mixtures, a new viscosity function was introduced. The code has been structured in a way that the gas component can be changed more easily in the future.

The following conclusions can be drawn from the test results:

- For a correct simulation of the dilation process, there should be at least a very small gas saturation in all elements, i.e. even in elements which are fully saturated with water. Gas saturation may be as low as 1E-10 and should not exceed the expected maximal porosity increase. However, even a small gas saturation may introduce significant amounts of dissolved gas in the system. Further research might be necessary to avoid this artificial effect.

- The modified code calculates the equilibrium between porosity and pressure, which is determined by the dilation relationship $\phi(p)$, correctly.

- Mass conservation during porosity change is very accurate. Relative errors of less than 1E-15 per time step with regard to the sum of the masses of water and brine and relative errors of less than 1E-13 per time step with regard to the mass of H_2 show the high precision of the implemented numerical routines.

- A wide time step causes a delay in the dilation response of an element to a pressure change. The delay is in the same order of magnitude as the width of the time step.

- A low grid resolution leads to numerical dispersion, which mainly affects the sharpness of the dilation front. In case of a gas injection, a low grid resolution leads to faster propagation of the dilation front and thus underestimates the pressures at the location of the gas injection. Except for this phenomenon, the implemented transport mechanism shows no marked grid-dependency.

- The automatic time step control provided by TOUGH2 does not allow an appropriate simulation of the dilation-controlled transport process. Time step widths were reduced by limiting the maximal absolute pressure change during a time step for dilated elements or for elements that will be dilated after completion of the time step. This proved to be sufficiently efficient. However, a more advanced time step control could be necessary in the future in order to speed up the calculations.

5 Application to a generic far-field model

The code TOUGH2-PD has been applied to a hypothetical German repository for radioactive waste with non-negligible heat generation in clay stone in order to investigate the pressure evolution in the repository and gas migration in the host rock. At the beginning, analytical considerations were made in order to identify pressure domains in which pathway dilation might be of relevance.

5.1 Estimation of pressure domains for pathway dilation

Whether pathway dilation takes place and whether gas is transported mainly by advection or diffusion depends on the hydro-mechanical state of the rock. A simple analytical estimation is presented in order to assess which type of transport process can be expected at a certain depth. Rigorous pressure thresholds for visco-capillary flow of the gas phase and pathway dilation are assumed for this purpose which should be considered as a strong simplification due to the gradual onset of both processes.

We consider isostatic conditions within the rock mass. Assuming that dilated pores are almost fully saturated with gas in accordance with the conceptual model, the criterion for the formation of macroscopic fractures is defined with reference to the gas pressure

$$p_{\mathrm{gas}} \geq \sigma_3 = \rho_{\mathrm{rock}}\, g\, z ,$$

where σ_3 is the minimal principal *total* stress, ρ_{rock} is the rock density, g is the gravitation acceleration, and z is depth below surface.

We define p_{dil} to be the gas pressure threshold for the dilation of the rock mass. Experiments show that p_{dil} is a few Mega-Pascals below σ_3 /NAG 02, MAR 05/. A linear dependency

$$p_{\mathrm{dil}} = \sigma_3 \beta \quad \text{with } \beta < 1,$$

is assumed in order to prevent p_{dil} from falling negative for low values of σ_3.

Visco-capillary transport of gas without dilation sets on if the gas phase is able to displace the water phase. This is possible if the gas pressure p_{gas} exceeds the hydraulic pressure p_{hyd} plus the gas entry pressure p_{entry}. With this, a pressure threshold p_{vc} for the visco-capillary flow of a gas phase without dilation is defined:

$$p_{\mathrm{vc}} = p_{\mathrm{hyd}} + p_{\mathrm{entry}} \quad \text{with } p_{\mathrm{hyd}} = \rho_{\mathrm{fl}}\, g\, z.$$

Both functions p_{dil} and p_{vc} can be used to delimit four pressure domains with different transport processes (Figure 5-1):

1. $p_{gas} < p_{dil}$ and $p_{gas} < p_{vc}$: In the absence of any advection, diffusion of dissolved gas is the dominant transport process for gas.

2. $p_{gas} > p_{vc}$ and $p_{gas} < p_{dil}$: The gas phase can displace water from the primary porosity and flow without creation of secondary porosity.

3. $p_{gas} > p_{dil}$ and $p_{gas} < p_{vc}$: The rock dilates due to the formation of secondary pore space. This allows the gas phase to flow in the secondary porosity before water can be displaced from the primary porosity.

4. $p_{gas} > p_{dil}$ and $p_{gas} > p_{vc}$: A gas phase may flow through primary and secondary pore space.

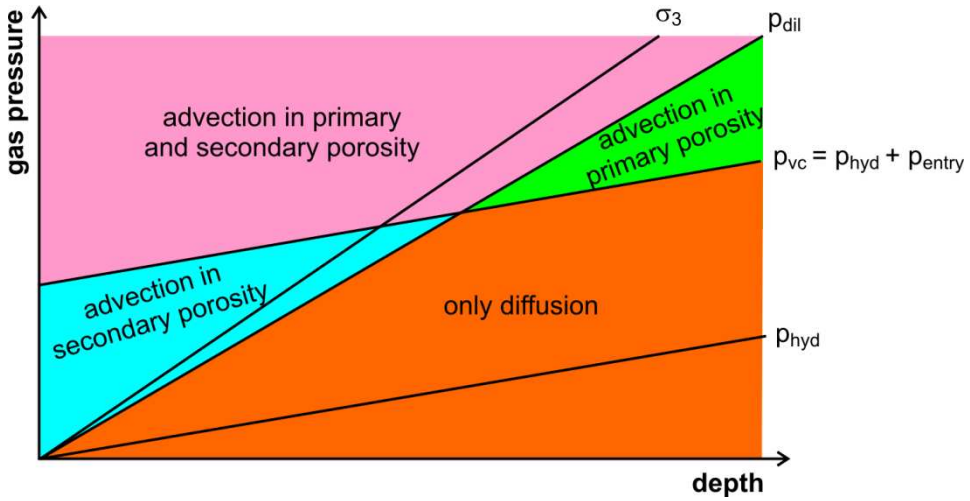

Figure 5-1: Schematic illustration of pressure domains for the flow in primary pore space (pore space before dilation) and secondary pore space (gained by dilation).

For a repository at depth z, upper and lower pressure limits for the gas pressure inside the repository shall be estimated. For this purpose, an initial state of the repository system has to be identified. This is not straight forward without explicit modelling of the processes leading to this state. Therefore the existence of a state is assumed in which the gas phase has not yet entered from the repository into the host rock and in which the pore saturation in the repository has dropped to the residual liquid saturation. Pressure within the adjacent host rock shall have fairly recovered to $p_{hyd}(z)$ at this time. There is also no overpressure in the host rock. For simplicity, the capillary pressure within the repository shall be 0 and the gas pressure inside the repository is assumed to be approximately equal to $p_{hyd}(z)$. (The pore water pressure in the host rock is $p_{hyd}(z)$ and thus the water and gas pressure inside the repository, which are equal, are in reality probably slightly higher than $p_{hyd}(z)$ in order to be consistent with the fact that repository water has escaped into the host rock.) The initial conditions for all of the following analytical and numerical considerations are defined according to this hypothetical state.

The minimal gas pressure in the repository is given by the initial condition $p_{lb} = p_{hyd}(z)$ (lb: “lower boundary”). Gas pressures will not drop below this pressure due to gas generation.

On the other hand, gas pressures inside the repository will not exceed the pressure that would arise if gas couldn't escape from the repository:

$$p_{\mathrm{ub}} = p_{\mathrm{hyd}}(z) + nRT / V_{\mathrm{storage}}$$

(ub: "upper boundary"), where n is the number of moles of generated gas, R is the universal gas constant, T is the absolute temperature and V_{storage} is the gas volume inside the repository, which is calculated by

$$V_{\mathrm{storage}} = V_{\mathrm{rep}} \phi_{\mathrm{rep}} (1 - S_{\mathrm{lr}}) .$$

We consider a repository located at a depth of 450 m below surface. When gas pressures rise, the pressure path will either pass the p_{vc} or p_{dil} curve first. The transport mechanisms that can be expected at a depth of 450 m will therefore depend on the depth of the intersection p_{vc} = p_{dil}. Keeping p_{dil} constant, two gas entry pressures will be considered which locate the intersection p_{vc} = p_{dil} 250 m below and 250 m above the repository depth. Thus, using the parameters given in Table 5-1, the entry pressures

$$p_{\mathrm{entry,1}} = 2.16 \text{ E+6 Pa} \quad \text{and} \quad p_{\mathrm{entry,2}} = 7.56 \text{ E+6 Pa}$$

will be considered. Figure 5-2 shows, that the upper boundary p_{ub} for the gas pressure inside the repository lies well above the thresholds p_{dil} and p_{vc}. This implies that on the basis of the chosen parameters, significant dilation and flow phenomena can be expected.

Table 5-1: Parameters for the estimation of pressure domains.

g	9.81	m/sec²
ρ_{fl}	1000.0	kg/m³
ρ_{rock}	2765.0	kg/m³
n	3.41 E+09	mol
R	8.314472	J mol^{-1} K^{-1}
T	298.15	K
β	0.76	
ϕ_{rep}	0.2	
S_{lr}	0.1	
V_{rep}	1 E+6	m³

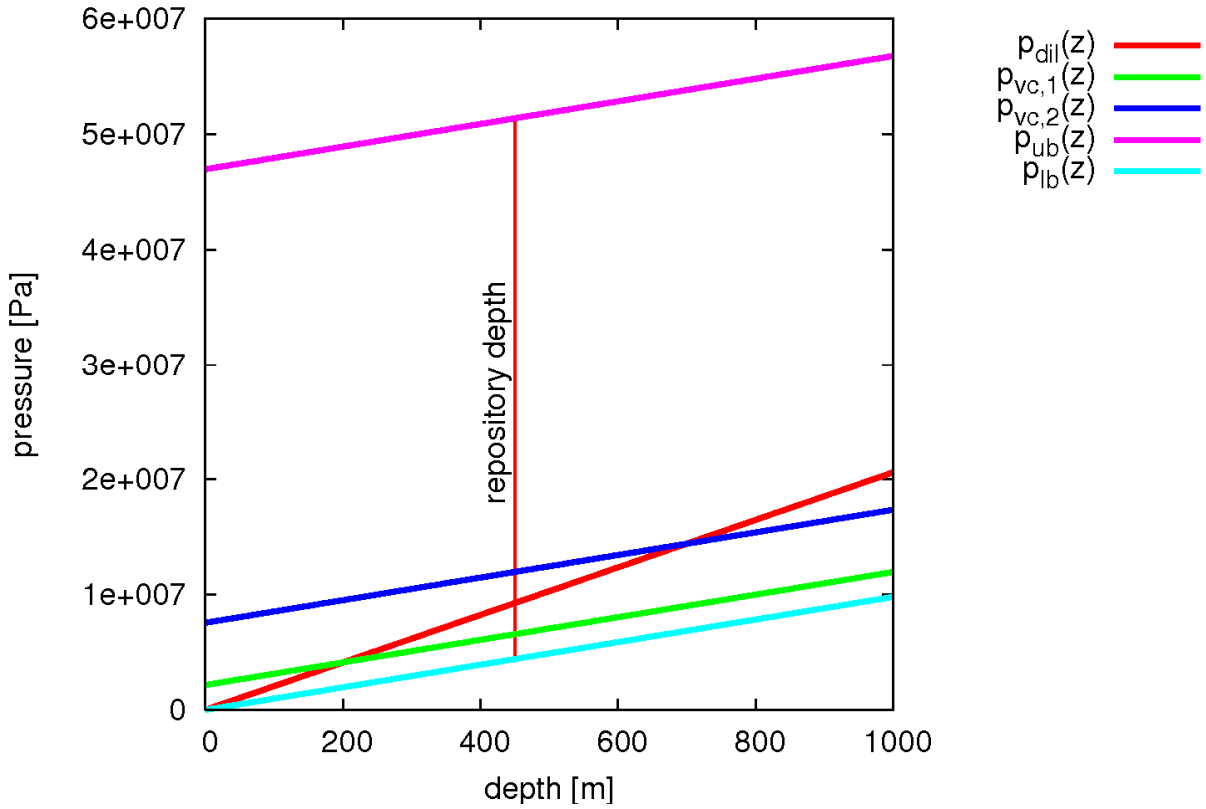

Figure 5-2: Boundaries for the gas pressure inside the repository. Two threshold pressures $p_{\mathrm{vc},1}(z)$ and $p_{\mathrm{vc},2}(z)$ are defined using the gas entry pressures $p_{\mathrm{entry},1}$ and $p_{\mathrm{entry},2}$, respectively.

5.2 Calculation cases

5.2.1 Geometrical model

We define a rectangular model domain representing a horizontal clay layer which is confined by aquifers to the top and to the bottom (Figure 5-3). The domain's height is 430 m, its lateral length is 2500 m × 1500 m or 4000 m × 3000 m depending on the considered simulation case. The repository – more precisely one quarter of the repository – is located in a vertical edge of the domain at a depth of 450 m. It has lateral lengths of 1 km (4 elements) by 2 km (8 elements). The repository's clay overburden amounts to 190 m.

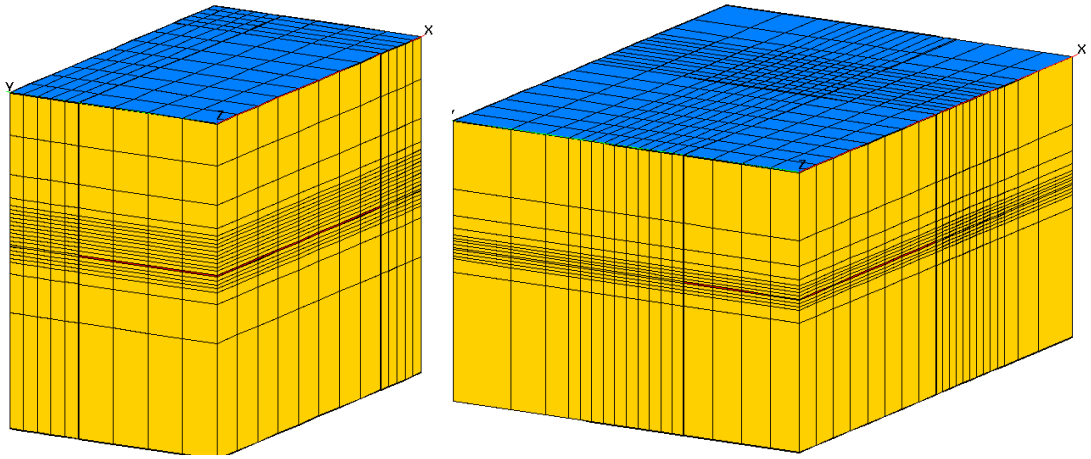

Figure 5-3: Model geometry. – Left: standard geometry, right: model geometry for case "2D". Vertical z-axis exaggerated by a factor of 5. Scales are in metres.

A special discretisation is used to describe the repository. According to the height of the emplacement caverns the repository height is set to 2.5 m. The repository is therefore contained in a rectangular domain of 8 km² × 2.5 m which partly consists of host rock and partly of repository caverns. A small layer with a dimension of 0.125 m × 8 km² is introduced to represent the caverns whose volumes sum up to 10^6 m³. This "cavern layer" is covered by another layer of host rock with a height of 2.375 m representing the host rock between the caverns. When gas is produced inside the repository, it will first escape from the cavern layer to the host rock layer at the top due to the pressure and stress gradients. The upwind weighting scheme for mobilities will cause a quick gas transfer between both layers which will therefore act as one unit. This type of discretisation minimises artificial effects arising from the upwind weighting scheme and allows a reasonable lateral homogenisation of emplacement galleries. Artificial effects on the lateral gas flow caused by the upwind weighting scheme are reduced by the introduction of very thin vertical layers at the lateral boundaries of the repository.

5.2.2 Boundary and initial conditions

To the top and to the bottom, the clay layer is confined by a thin layer of inactive elements which define fixed pressure boundaries (aquifers). There is no difference in the hydraulic potential between the upper and lower boundary, i.e. no leakage. All lateral boundaries are no-flow boundaries, either being far away boundaries or symmetry planes. All simulations start with an equilibrated hydraulic state.

5.2.3 Case-specific code modifications

Single-phase states may cause numerical problems in TOUGH2 simulations and will most likely occur in repository elements because the gas pressure forces the pore water to escape

into the host rock. To avoid single-phase states in the repository, the mobility for water is set to zero for all element connections with at least one repository element.

Special attention has to be paid to the simulation of H_2-diffusion out of the repository due to the very low liquid saturation inside repository elements. For fully desaturated elements, TOUGH2 calculates the dissolution of H_2 in a hypothetical small liquid volume. In principle this would allow to simulate diffusion within the liquid phase even for fully desaturated elements. However, effective diffusivities for the liquid phase calculated by TOUGH2 would vanish for vanishing liquid saturation due to tortuosity effects. This underestimates the diffusive flow of dissolved H_2 out of the strongly desaturated repository since the dissolution of H_2 across the repository-clay-interface is neglected by TOUGH2. Therefore eq. (3) is replaced by a new formulation for the effective diffusivity:

$$D_{\mathrm{eff,liq}}^{\mathrm{H2}} = \phi^{4/3}{}_{\mathrm{host\,rock}} d_{\mathrm{liq}}^{\mathrm{H2}} .$$

This formulation is based on the Millington-Quirk model assuming $S_{\mathrm{liq}} \approx 1$. Hereby, diffusion of H_2 out of the repository is now controlled by the properties of the host rock.

5.2.4 Reference case

The reference case is parameterised according to Table 5-2 while assuming isothermal conditions. The liquid is composed of water and dissolved H_2, the gas phase contains H_2 and vapour. There shall not be any brine in the domain. Inside the repository, there is a time dependent gas source whereas gas generation is estimated on the basis of a container concept developed in BMU-project SR 2438 for German radioactive wastes with non-negligible heat generation (see Table 5-2).

Dilation parameters of the host rock are derived from data presented in /NAG 02/. In the gas-threshold-pressure-test O5 implemented in the Benken borehole, dilation-induced gas transport was noticed to occur approx. 3 to 4 MPa below the minimal principal stress σ_{min} which was about 14 to 15 MPa. The threshold for dilation is therefore set to 0.76 σ_{min}, i.e. β = 0.76. Numerical analysis of the O5 test suggested a permeability increase by a factor of 2 to 5 approximately 1 MPa above the dilation threshold. It was therefore assumed here that gas permeability parallel to the bedding plane increases linearly with pressure with a gradient of 1.65 E-20 m² MPa^{-1} which is 5 times the intrinsic permeability parallel to the bedding plane per 1 MPa. Long-term gas tests in the FM-niche and at the GS-site /NAG 02/ showed mechanical deformations up to 30 µm/m. Assuming that these deformations only attribute to the creation of micro-cracks this indicates a porosity increase of about 0.0001. Therefore a porosity increase of 0.0001 MPa^{-1} above the dilation threshold was assumed, which is very small compared to the porosity of the rock. It has to be noted that there are large uncertainties connected to this parameterisation.

Two-phase flow parameters for clays are difficult to obtain experimentally for high liquid saturations. In order to avoid severe desaturation when gas enters the saturated clay a modified version of the van Genuchten capillary pressure function $p_{c,vanGen}$ /PRU 99/ is used. The modified capillary pressure function is defined by $p_c=\max(p_{c,vanGen}, p_{entry})$ for liquid saturations below $S=S_e$, and by a linear decrease to 0 in the interval $S=S_e$ to 1 (see Figure 5-4). S_e is the maximum liquid saturation with $p_c=p_{entry,}$ and is set to 0.98 in the reference case.

Table 5-2: Parameters and reference values for the reference case

General		
Magnitude of the gravitational acceleration vector	g	9,81 m/sec^2
Temperature (isothermal conditions)	T	298.15 K
Components		
	Pure water and H_2. No brine.	
molar mass of H_2	m_{air}	2.016 g/mol
molar mass of water	m_{water}	18.016 g/mol
Phases		
	Liquid (water, dissolved H_2) and gas (H_2, Vapour)	
Klinkenberg parameter	β	0 Pa
Repository		
Depth		450 m
Area (only ¼th is simulated)		8 km²
Height		2.5 m
Volume of excavated caverns		1 E+06 m³
Total H_2 generation rate (only ¼th is simulated)		
year 0 to 82760		2.3 E-06 kg/s
year 82800 to 91200		1.6 E-06 kg/s
year 91200 to 94500		1.3 E-06 kg/s
year 94500 to 102500		1.16 E-06 kg/s
year 102500 to 482400		1.33 E-09 kg/s
total amount of H_2		3.41 E+09 mol

Domains		Clay	Repository
Actual porosity		0.10	0.2
"Intrinsic" or "absolute" permeability			
in x-direction (|| to bedding plane)	k_x	$3.3 \cdot 10^{-21}$ m^2	$1 \cdot 10^{-18}$ m^2
in y-direction (|| to bedding plane)	k_y	$3.3 \cdot 10^{-21}$ m^2	$1 \cdot 10^{-18}$ m^2
in z-direction ($\perp$ to bedding plane)	k_z	$6.6 \cdot 10^{-22}$ m^2	$1 \cdot 10^{-18}$ m^2
Diffusion			
New model for effective diffusivity to allow diffusion out of repository: $D^{H2}_{eff,liq} = \phi^{4/3}_{rock} d^{H2}_{liq}$			
diffusion coefficient of H_2 in gas at ref. state	$d_{gas}^{H2}(p_0, T_0)$	0	same
diffusion coefficient of vapour in gas at ref. state	$d_{gas}^{vapour}(p_0, T_0)$	0	same
diffusion coefficient of water in liquid		0	same
Effective diffusion coefficient of H_2 in water	$D^{H2}_{eff,liq}(p, T)$	$1 \cdot 10^{-11}$ m^2/s	same
$\Rightarrow$ diffusion coefficient of H_2 in water (assumed experimental conditions: ϕ=0.1, S=1, p=1 atm=1.01325 bar and T = 25 °C, see eq. 9)	$d_{liq}^{H2}(p_0, T_0)$	$2 \cdot 10^{-10}$ m^2/s	same
no pore compressibility, no thermal pore expansivity			
relative permeability function: Corey curves according to Pruess (1999)			
residual liquid saturation		0.2	0.1
residual gas saturation		0	0
capillary pressure function		Modified van	No capillary pressure
Modified van Genuchten-Mualem function: p_c does not drop below p_{entry} except for the range $S_e < S_l < 1$ where p_c drops linearly to 0.			
apparent gas entry pressure	p_{entry}	7.56 MPa	
highest liquid saturation with $p_c = p_{entry}$	S_e	0.98	
residual liquid saturation	S_{lr}	0.1	
maximum liquid saturation	S_{ls}	1	
	λ	0,43	
maximum capillary pressure	$p_{cap,max}$	100 MPa	

Initial conditions		Clay	Repository
Minimal stress (constant) m/sec²	$\sigma_3(z) = z$ · 2765 kg/m³ · 9.81 m/sec²		
Liquid pressure	$p(z) = z$ · 1000 kg/m³ · 9.81		
Gas saturation	S_g	1E-06	0.90
Brine saturation (no brine)	S_b	0	0
Temperature (constant)	T	25 °C	25 °C
Stress conditions			
rock grain density	ρ_{grain}	2765 kg/m^3	same
Minimal principal stress	σ_{min}	$r_{grain}\, g\, z$	
Fracture system 1			
Applied to domain …		host rock	
threshold pressure for dilation	p_{thr}	0.76 s_{min}	
Porosity due to dilation $\phi(p)$ (see equation (25) in /NAV 08/)			
Porosity change in pressure interval Δp_ϕ	$\Delta\phi$	0.0001	
	Δp_ϕ	1 MPa	
Max. porosity change		no limit	
Gas permeability $k_{dil}(p)$ (see equation (24) in /NAV 08/)			
Permeability change in pressure interval Δp_k	Δk_{dil}	1.65 E-20 m² = 5 x intrinsic perm || to bedding plane	
	Δp_k	1 MPa	
Exponent	α	2	
Max. gas permeability		no limit	
Permeability tensor	$\mathbf{K}$	$\begin{pmatrix} 1 & 0 & 0 \\ 0 & 1 & 0 \\ 0 & 0 & r_i \end{pmatrix}$	
Isotropy ratio (vertical gas permeability / horizontal gas permeability)	r_i	0.1	
Simulation parameters and additional assumptions			
Start of simulation (t=0)	Beginning of gas production		
End of simulation	500,000 years later		
Permeability weighting		harmonic	
Mobility weighting		upstream	
Special assumptions for the liquid phase in the repository		Zero mobility of liquid phase for host rock/repository connections to avoid single phase states inside the repository	

5.2.5 *Alternative cases and gas entry models*

Additional to the reference case, 17 calculation cases were defined by varying one or two parameters versus the reference case. The specification of each case relative to the reference case is given in Table 5-3.

Table 5-3: Calculation cases

Subject of variation	**Description**	**Difference to reference case**	**Case Name**
	Reference Case	No difference	Ref
All dilation properties	No dilation	Dk_{dil}=0, Df=0	NoDil
Capillary pressure	Van Genuchten capillary pressure function	p_c according to van Genuchten (Pruess 1999)	VanGen
	low gas entry pressure	p_{entry} = 2.16 MPa	LoEntryPres
	Rigorous threshold behaviour for gas entry	S_{entry} = 0.999	RigThres
Relative gas permeability	Van Genuchten capillary pressure function with zero gas flow if $p_c<p_{entry}$.	p_c according to van Genuchten, $S_{r,gas}=S(p_c=p_{entry})$	FlowThres
	No dilation. Van Genuchten capillary pressure function with zero gas flow if $p_c<p_{entry}$.	p_c according to van Genuchten, $S_{r,gas}=S(p_c=p_{entry})$	FlowThresNoDil
Anisotropy of gas permeability	No Anisotropy	r_i= 1	Iso
	Very strong	r_i = 0	2D
	Strong	r_i = 0.0001	HiAniso
Primary porosity of clay	high	f = 0.2	HiPrimPor
	low	f = 0.05	LoPrimPor
Secondary porosity (dilated pathways)	High	Df = 1E-2	HiSecPor
	Low	Df = 1E-6	LoSecPor
Gas permeability of dilated pathways	High	Dk_{dil} = 50 x intrinsic permeability	HiGasPerm
	Low	Dk_{dil} = 0.5 x intrinsic permeability	LoGasPerm
Exponent of gas permeability	Low	a = 1	LoExp
	High	a = 3	HiExp

5.2.6 Remark on gas entry models

According to chapter 5.1, gas entry pressures of 2.16 MPa and 7.56 MPa are used in the simulation cases. However, there are different ways of implementing gas entry pressures, which will be explained in the following.

Simulating gas entry thresholds in the context of two-phase flow theory

From the perspective of the two-phase flow theory, a gas entry event may have two different reasons. The first reason may be that the relative permeability of the gas phase suddenly increases from zero to significant values during desaturation thereby giving the gas phase the ability to flow. This will likely happen if the porous medium has a non-zero residual gas saturation S_{rg} for which the relative gas permeability is zero if $S_{liq} > 1\text{-}S_{rg}$. Starting from the saturated state with zero capillary pressure, the gas phase will be able to flow as soon as the absolute value of the capillary pressure exceeds the value $|p_{cap}(1\text{-}S_{rg})|$. Consequently, $|p_{cap}(1\text{-}S_{rg})|$ defines a gas entry pressure. This is a possible way to introduce gas entry thresholds as ***mobility thresholds*** as it was done e.g. in /CRO 06/. There is some degree of freedom in how gas entry pressures can be introduced in this way because the same gas entry pressure can be defined with different values of the maximum liquid saturation $1\text{-}S_{rg}$ as long as $p_{cap}\,(1\text{-}S_{rg}) := -p_{entry}$. Thus, different combinations of capillary pressure and relative gas permeability functions may be used to introduce a certain gas entry pressure. However, it has to be noted that different combinations will differ with regard to the liquid saturation $1\text{-}S_{rg}$ achieved at the point of gas entry which may have an effect on the gas migration process.

The second possible reason for a gas entry event is connected to the properties of the capillary pressure function. Some capillary pressure – saturation curves (e.g. the van Genuchten curve) show a steep inclination at high liquid saturations when a log-scale is used and a moderate inclination for intermediate liquid saturations. This means that increasing the absolute value of the capillary pressure (starting from zero) will lead to a slight desaturation in the beginning which is followed by a sudden desaturation as soon as the capillary pressure – saturation state moves to the region of the capillary pressure curve which has a lower inclination (in this region, small changes of capillary pressure will lead to considerable changes of liquid saturation). Such a desaturation event increases the storage capacity for the gas phase and the relative gas permeability, and will thus be noticed as a gas entry event. (This process requires that the gas phase is already mobile.) The capillary pressure function therefore may define a gas entry threshold which basically is a ***desaturation threshold***, because the capillary pressure function does not control the mobility of the phases directly. The “entry pressure” parameter of the van Genuchten capillary pressure function is an example for such a desaturation threshold.

Porous media may show both, desaturation thresholds and mobility thresholds, depending on the constitutive two-phase flow relations in use. Mobility thresholds are always present if $S_{rg}>0$, and in this case $|p_{cap}(1\text{-}S_{rg})|$ defines the respective threshold pressure. Desaturation thresholds are present if the capillary pressure curve shows regions of decreased inclination

and the respective threshold pressures (there may be more than one) are the absolute capillary pressures at the beginning of these regions (if moving forward on a desaturation path). Actually, desaturation of a porous medium requires mobility of the gas and the liquid phase, so that desaturation thresholds should only be effective if their threshold pressure lies above the mobility threshold pressure, i.e. if $S_{liq}(p_{entry}) < 1\text{-}S_{rg}$. However, this can be different for discrete numerical models which use e.g. an upwind weighting scheme for the phase mobility. In this case, a grid element in which $S_{liq} > 1\text{-}S_{rg}$ will be able to desaturate if there is an adjacent grid element with a mobile gas phase at higher gas pressure. Whether such a mobility of the gas phase for $S_{liq} > 1\text{-}S_{rg}$ is physically plausible has to be answered on the basis of experimental evidence.

Choice of constitutive two-phase flow relations

Figure 5-4 shows the capillary pressures and relative gas permeabilities used in cases Ref, RigThres, LoEntryPres, VanGen, and FlowThres to account for gas entry. This has been done in three different ways:

- Case VanGen is characterised by non-vanishing relative gas permeabilities for the unsaturated state ($S_{rg}=0$) and the van Genuchten function is used to describe capillary pressures. Thus, there is no mobility threshold but a desaturation threshold for gas entry. Case VanGen permits a desaturation of over 20% for a gas pressure $p_{gas}=p_{hyd}+p_{entry}$ (p_{entry} is a parameter of the van Genuchten function).

- Cases Ref, RigThres, and LoEntryPres are characterised by the same relative permeability function as case VanGen but a modified van Genuchten function for capillary pressures. Capillary pressures lie below the van Genuchten parameter p_{entry} only for very high liquid saturations (> 98 %). (Note that p_{entry} takes a different value in the LoEntryPres case.) Thus, in simulation cases where gas pressures remain below the gas entry pressure, desaturation of the clay will be very low (< 2%). The chosen constitutive two-phase relations define a desaturation threshold but no distinct mobility threshold. However, due to the gradual increase of the relative gas permeability function, the gas mobility for liquid saturations $S_{liq} > 0.98$ is very small.

- FlowThres and FlowThresNoDil use the standard van Genuchten capillary pressure function but the residual gas saturation S_{rg} of the relative permeability function is non-zero and set so that $|p_{cap}(1\text{-}S_{rg})| = p_{entry}$ and gas permeabilities vanish for gas pressures $p_{gas}<p_{hyd}+p_{entry}$. This defines a mobility threshold for gas entry.

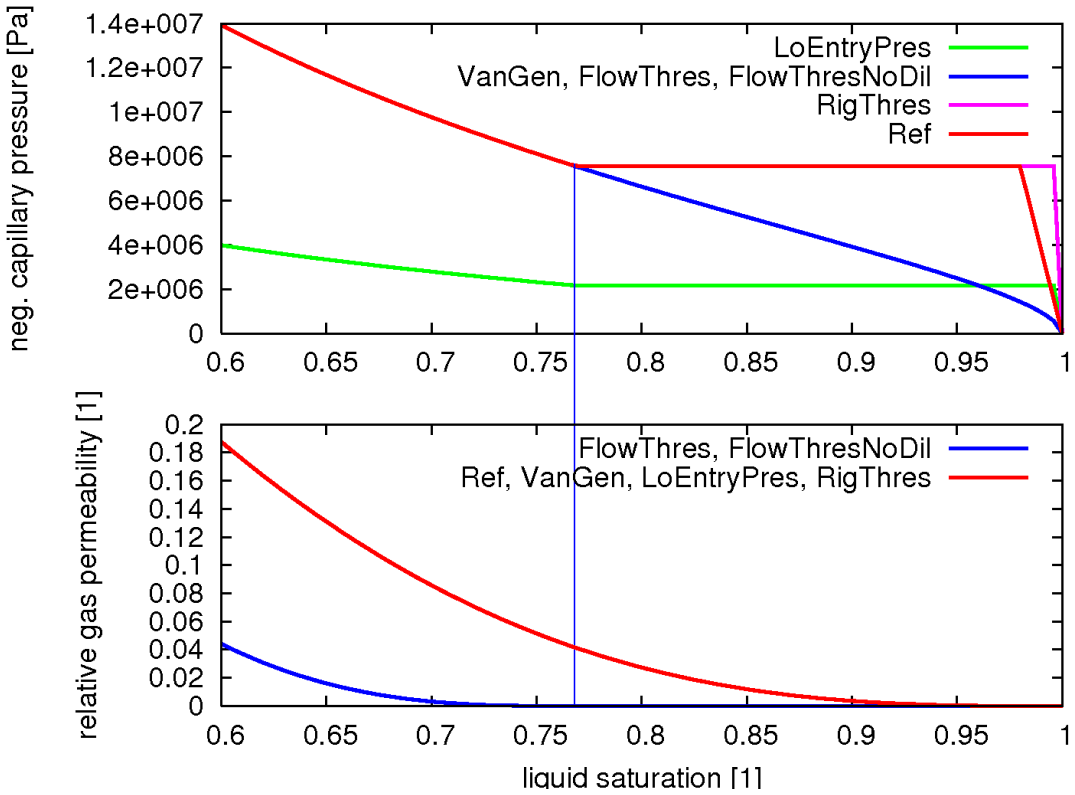

Figure 5-4: Capillary pressure and relative gas permeabilities functions used for the simulation of different gas entry behaviour.

5.3 Simulation Results and Interpretation

5.3.1 Gas pathways and shape of the dilation zone

Figure 5-5 shows the gas saturation after 100,000 a, i.e. at the end of the phase of elevated gas generation rates. Figure 5-6 shows the distribution of the secondary porosity, which illustrates the extent of the dilation zone. The isotropy ratio r_i for the cases Iso, Ref, HiAniso, and 2D displayed in the figures is equal to 1, 0.1, 0.001, and 0, respectively. The extent of the desaturated zone exceeds that of the dilation zone because the relative permeability function defines no physical gas entry pressure in the considered cases (S_{rg}=0).

Cases Ref and Iso do not show any lateral propagation of the gas phase. There is a relatively slight horizontal propagation of the gas phase in case HiAniso but the vertical movement of the gas phase is predominant. Only in case 2D (where the vertical gas permeability of the secondary pore space is set to 0), the horizontal propagation of the gas phase exceeds the vertical propagation. The distribution of the secondary porosity which displays the propagation of the dilation zone is quite similar (Figure 5-6). Vertical propagation is predominant in cases Iso, Ref, and HiAnis, whereas horizontal propagation is predominant

in case 2D. It has to be noted that the lateral extent of the dilation zone probably depends on the height of the repository which is 2.5 m in all cases.

The fact that a strong anisotropy of the gas permeability is needed to achieve a horizontal propagation of the dilation zone can be explained by the depth-dependency of the minimal principal stress. The propagation of the dilation zone is controlled by the dilation thresholds at the dilation front. In case of an upward propagation of the front, these thresholds decrease continuously since they are linearly dependent on the minimal principal stress. In case of a horizontal propagation of the dilation front the dilation thresholds remain constant. All in all, this favours a vertical propagation of the dilation zone.

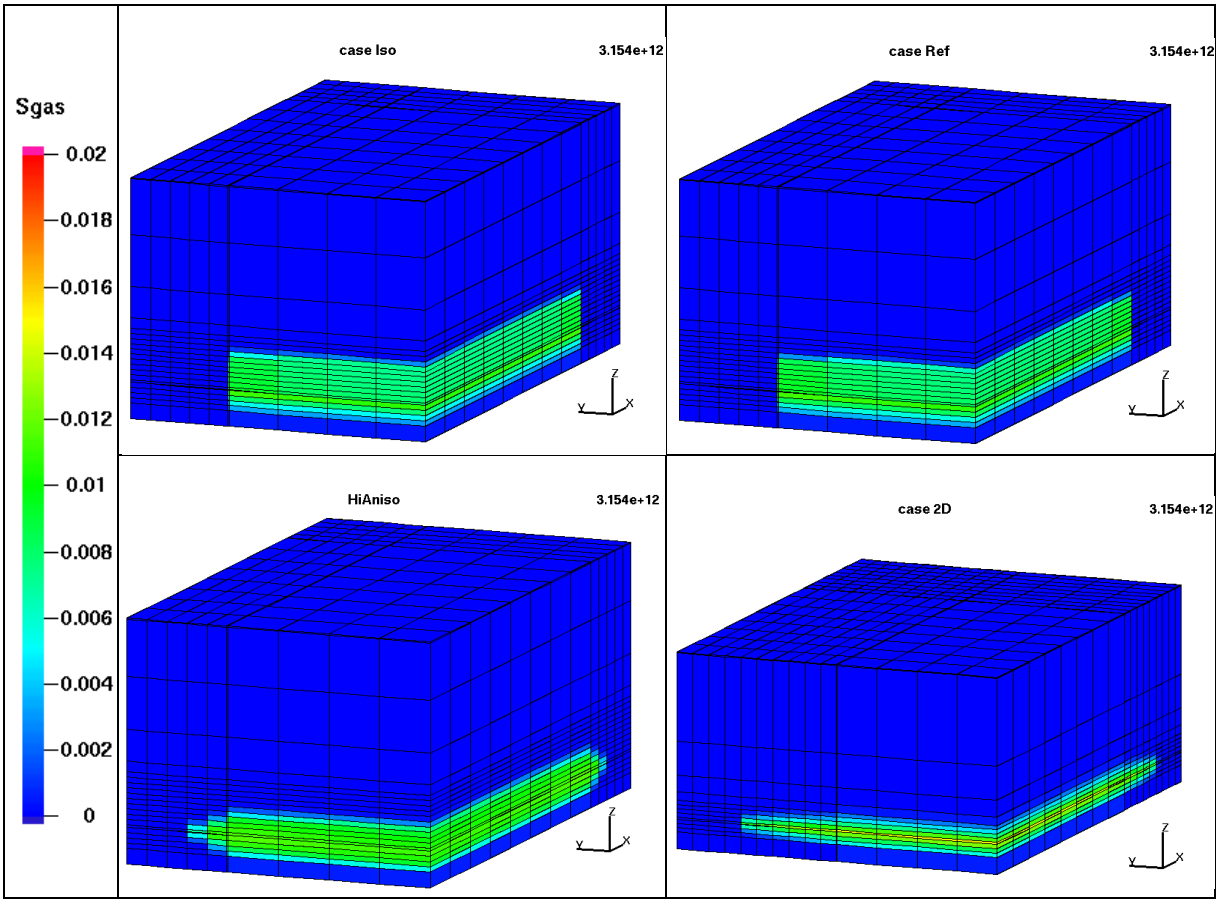

Figure 5-5: Gas saturation in the vicinity of the repository. – The represented part of the repository has an extent of 1 km in y-direction (4 elements) and of 2 km in x-direction (8 elements). The model has been cropped in the direction of the negative z-axis. The z-axis is exaggerated by a factor of 5.

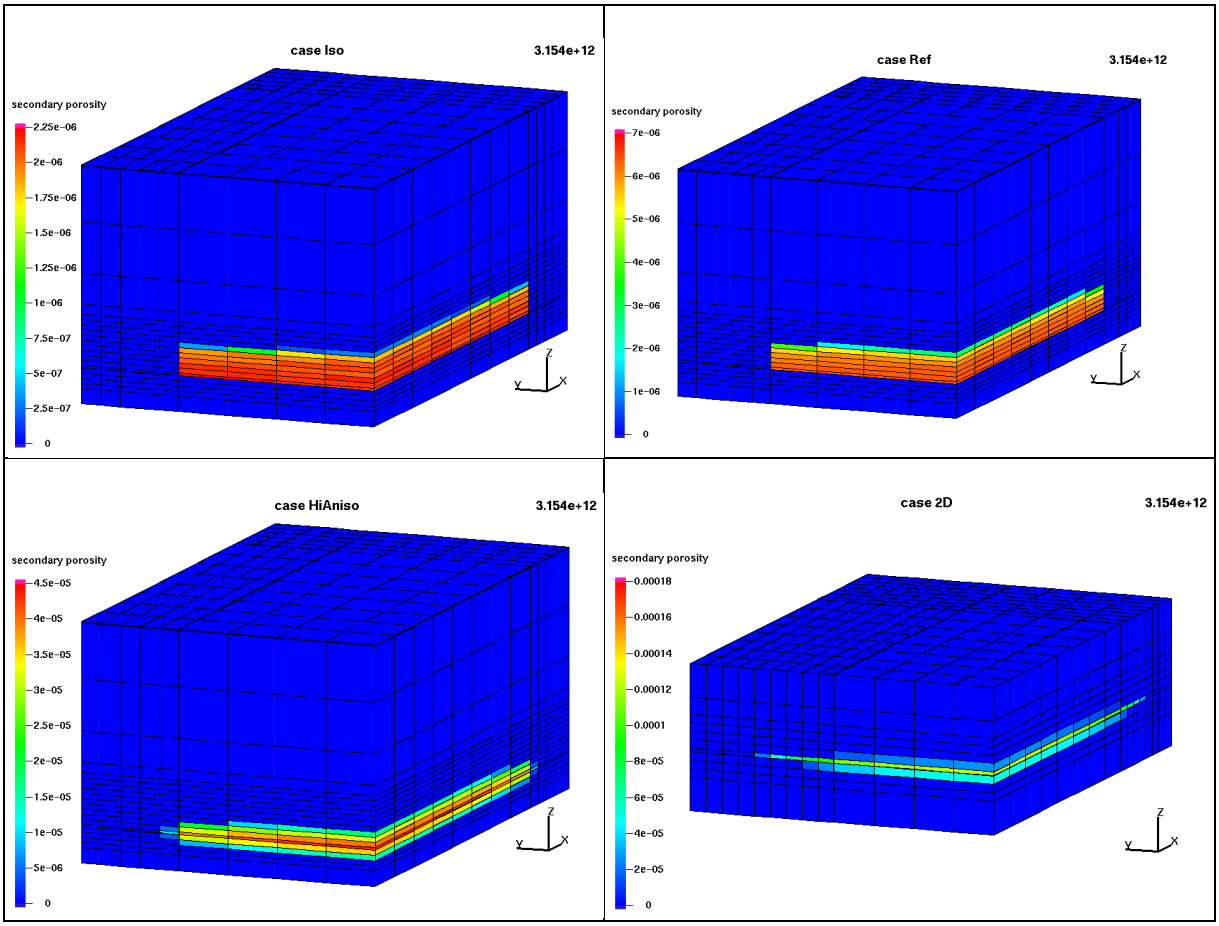

Figure 5-6: Secondary porosity in the vicinity of the repository. – The represented part of the repository has an extent of 1 km in y-direction (4 elements) and of 2 km in x-direction (8 elements). The model has been cropped in the direction of the negative z-axis. The z-axis is exaggerated by a factor of 5.

5.3.2 Pressure evolution

Figure 5-7 shows the evolution of the gas pressure inside the repository for the period from 0 a to 200000 a and compares it to the threshold pressure for dilation and macro-fracturing at repository depth which is 9.3 MPa and 12.3 MPa, respectively. For clarity, the results of the calculation cases are displayed in three separate diagrams using the same scaling.

In all cases with pathway dilation, gas pressure in the repository stays below the dilation threshold up to year 25000 and from year 127000 on. Maximum pressures are reached at about 90000 a. Macro-fracturing takes place only in case “NoDil” which does not account for dilation effects (Figure 5-7 bottom). In this calculation case, one single element layer at the bottom and at the top of the repository layer suffers macro-fracturing (Figure 5-8). However, space discretisation in z-direction is too coarse to determine the volume of rock subjected to macro-fracturing. In all other calculation cases, there isn’t any macro-fracturing, neither at

repository depth nor at any other depth, indicating that the process of pathway-dilation efficiently inhibits the evolution of macro-fractures.

According to the prediction no dilation takes place if the gas entry pressure is as low as 2.16 MPa ("LoEntryPres"), i.e. that the gas pressure at the point of gas entry ($p_{hyd}+p_{entry}$=4.41 MPa) is below the dilation threshold (9.31 MPa).

Figure 5-7 shows that the most important parameters influencing the gas pressure evolution are

- the anisotropy of the gas permeability caused by dilation (compare cases Ref, HiAniso, and 2D),
- the character of the capillary pressure function (compare cases Ref, VanGen, LoEntryPres, RigThres), and
- the primary porosity (compare cases Ref, LoPrimPor, HiPrimPor).

The maximum pressure which is observed in the repository increases with decreasing isotropy and decreasing primary porosity. It also increases if a modified van Genuchten function is used, i.e. if capillary pressures rise more quickly in the course of desaturation.

In cases FlowThres and FlowThresNoDil, in which the threshold for gas entry is simulated via a threshold for gas flow, a similar pressure evolution as case VanGen can be observed (Figure 5-7 bottom). This shows that the evolution of the gas pressure is much more affected by the capillary pressure functions than by the pressure threshold for advective inflow of the gas phase into the saturated clay which is controlled by the used relative permeability function.

An *increase* of isotropy (Iso) in relation to the reference case has only minor effect on the pressure evolution inside the repository. This also applies to the specific pressure-dependency of the gas permeability (LoGasPerm, HiGasPerm, LoExp, HiExp) and of the secondary porosity (LoSecPor, HiSecPor).

The pressure increase with decreasing isotropy can be explained by the fact that the dilation thresholds remain high in case of horizontal propagation of the dilation zone and the flow cross-section between repository and host rock is smaller than in case of a vertical zone propagation. These two factors hinder the flow of gas out of the repository with the consequence that gas pressures rise more quickly.

The effects of the primary porosity and of the capillary pressure function on gas pressure evolution probably attribute to the fact that these two material properties control the storage capacity of the rock for a gas phase. The storage capacity increases with increasing primary porosity. It also increases if the capillary pressure function changes in a way that allows a stronger desaturation of the rock. With a low storage capacity the gas phase has to be

distributed over a larger volume of rock which implies longer migration distances and higher pressures inside the repository in order to establish such a migration.

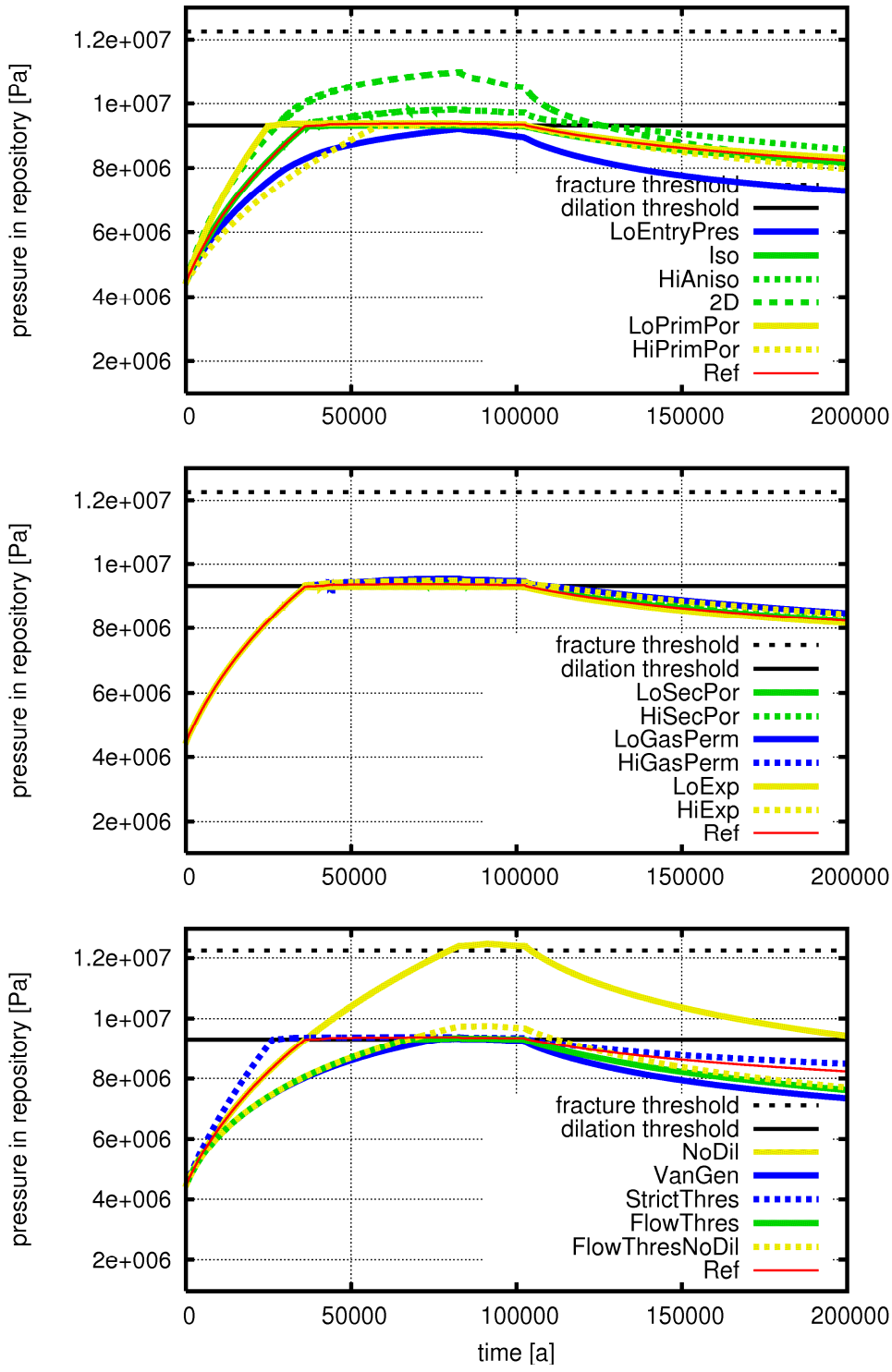

Figure 5-7: Pressure evolution in the repository. The upper and lower horizontal lines are the fracture and dilation thresholds at repository depth, respectively.

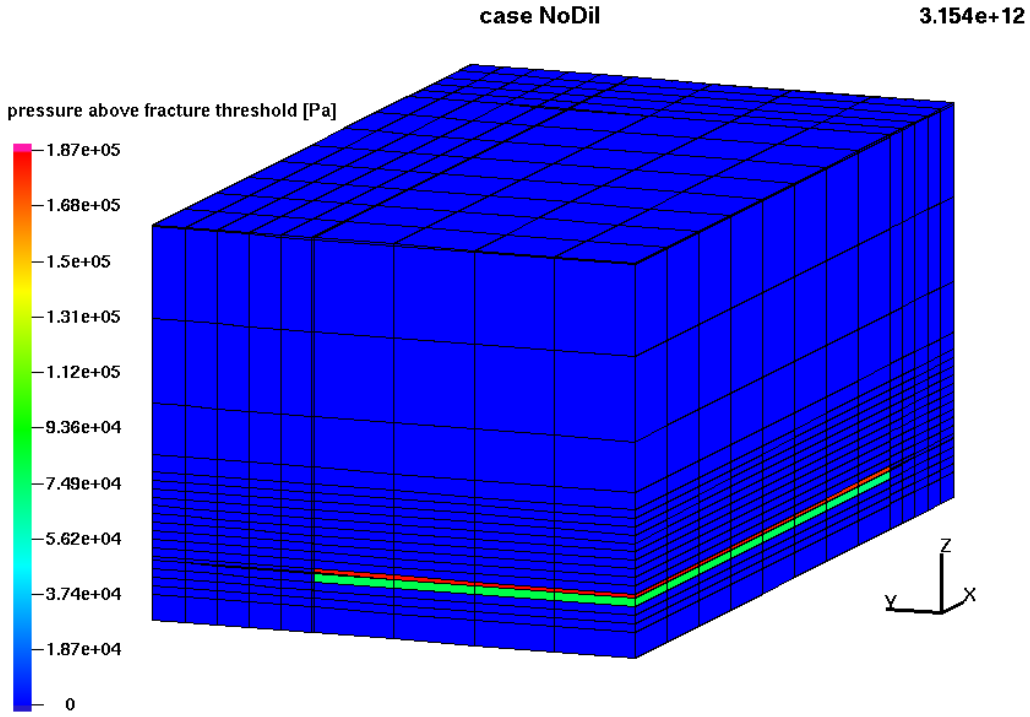

Figure 5-8: Domain of macro-fracturing at time 100,000 a in case “NoDil”. – The model has been cropped in the direction of the x-, y-, and negative z-axis, but the whole clay overburden of the repository (190 m) is displayed. The z-axis is exaggerated by a factor of 5.

5.3.3 Rock volume subjected to dilation

The extent of the dilation zone can be quantified by the volume of dilated grid elements representing host rock. Figure 5-9 illustrates the volume evolution of the dilation zone. All curves show a step characteristic which attributes to the given space discretisation. Because there was a tendency to oscillations in cases Iso, LoGasPerm, LoExp, HiSecPor, abd HiExp, these cases were performed with reduced time-step sizes.

Figure 5-9 (top) shows that the maximum volume of the dilation zone increases with

- increasing isotropy of the gas permeability (compare cases Ref, HiAniso, 2D),
- decreasing primary porosity (compare cases Ref, LoPrimPor, and HiPrimPor), and
- a more rapid increase of capillary pressures during desaturation (compare cases Ref, VanGen, FlowThres, RigThres).

The life-time of the dilation zone increases with

- increasing secondary porosity (by 55600 a in case HiSecPor),
- decreasing isotropy of the gas permeability (by 23800 a in case HiAniso, and by 20800 a in case 2D), and
- a more rapid increase of capillary pressures during desaturation (by 33800 a in case RigThres).

Minor delays of 7150 a and 7800 a can be noticed in case HiExp and LoGasPerm, respectively.

Apparently, the maximum volume of the dilation zone has the same sensitive parameters as the pressure evolution inside the repository. The increase of the dilation zone volume with increasing isotropy can be explained by the fact that the upward propagation of the dilation zone is facilitated by a continuous decrease of dilation thresholds. Additionally, the dilation zone grows faster if the storage capacity for a gas phase is small because the gas phase has to be distributed over a larger rock volume. The observed influence of the primary porosity and of the capillary pressure function on the volume of the dilation zone can therefore be explained by their influence on the storage capacity for a gas phase.

5.3.4 Gas storage

H_2 is stored either in dissolved or gaseous form. Because water is present only in the primary porosity according to the conceptual model, there are three H_2-fractions to distinguish:

- Dissolved H_2 in the primary porosity,
- Gaseous H_2 in the primary porosity, and
- Gaseous H_2 in the secondary porosity.

Figure 5-10 shows the mass of H_2 for these three kinds of storage.

In all cases the relative amount of H_2 in the secondary porosity is very small (10^2 to 10^4 times smaller than the gaseous fraction in the primary porosity) which attributes to the very small porosity increase due to dilation. Thus, the gas phase is predominantly stored in the primary porosity. It can be concluded from this that the capillary pressures, which have immediate influence on desaturation, have a stronger effect on the storage capacity of the rock for a gas phase than the porosity increase due to dilation. The dominant control of the storage capacity for a gas phase by the capillary pressures can be seen in the cases VanGen, LoEntryPres, FlowThres and FlowThresNoDil, which use capillary pressure functions that deviate from the reference case. Apparently, a decrease of capillary pressures at high liquid saturations leads to a stronger desaturation and thus to a higher fraction of gaseous H_2.

The relatively high H_2-fraction in solution shows that gas saturation is very small in all calculation cases. The noticed sensitivity of the capillary pressure is therefore related to the characteristics of the capillary pressure function at high liquid saturation.

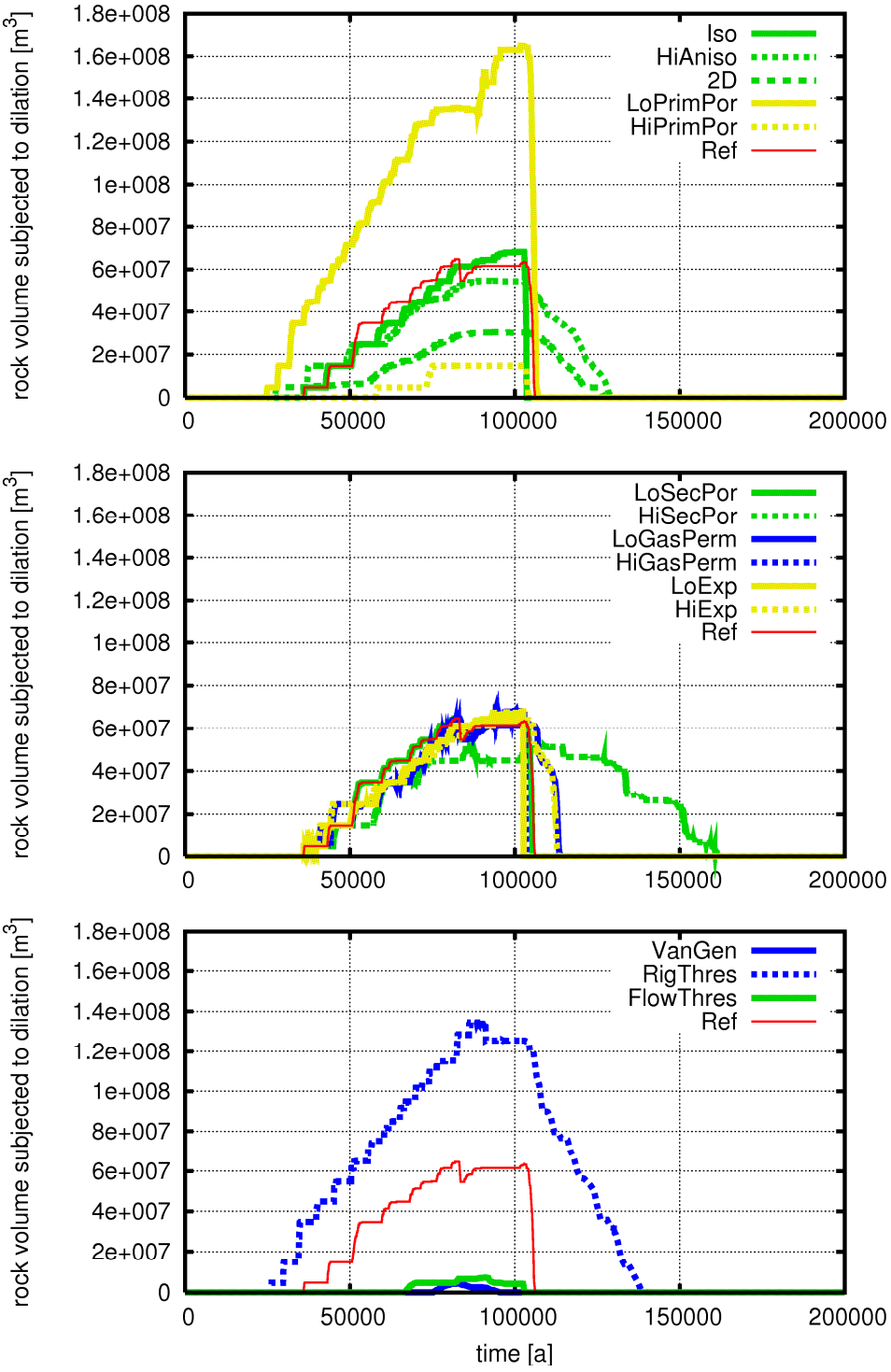

Figure 5-9: Evolution of the rock volume subjected to dilation.

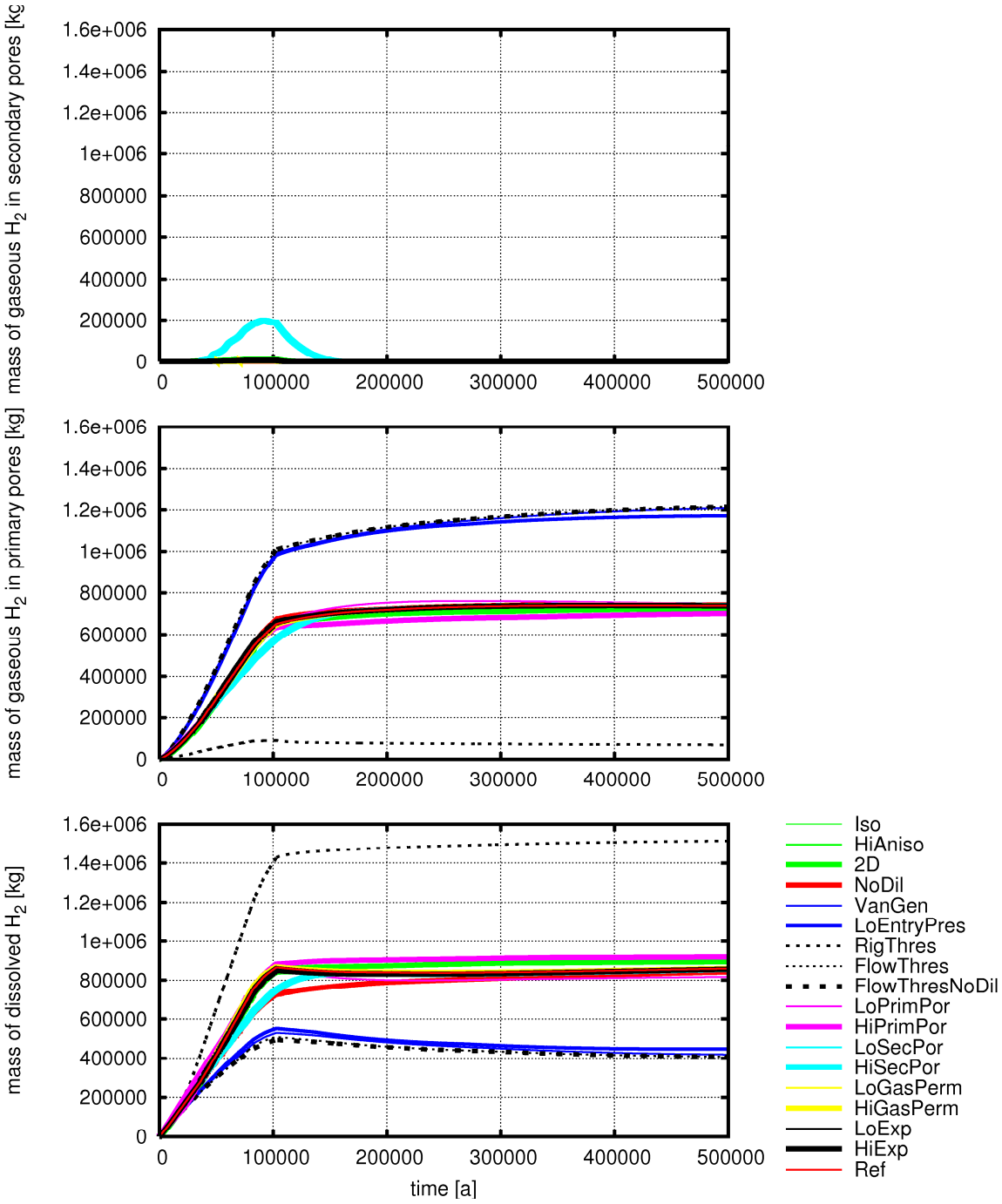

Figure 5-10: Mass distribution of dissolved and volatile H_2 (same scaling of plots).

6 Conclusions

The code TOUGH2/EOS7 has been modified to account for the mechanism of pathway dilation in clay stones with very low permeability. This code was named TOUGH2-PD (TOUGH2 with pathway dilation). A pressure-dependent porosity has been introduced in order to allow a gas phase to flow without need to displace the liquid phase. Whether desaturation and water displacement takes place or not is strongly influenced by the constitutive two-phase flow relations which are used. The TOUGH2-PD code does not exclude displacement of water by the gas phase but it is able to handle cases where such a displacement is difficult e.g. due to no-flow boundary conditions or very rigorous gas entry thresholds.

Porosity increase was modelled separately from the porosity-change-feature of TOUGH2 which affects the fluxes but not the storage capacity of the rock. Gas permeability was defined by adding a pressure-dependent gas flux within the secondary porosity (created by dilation) to the gas flux in the primary porosity. Liquid permeability is not affected by the dilation process because the dilated pore space is thought to be created and used mainly by the gas phase. This also aims at reproducing the observation of low water displacement in gas migration experiments. The approach of separate gas fluxes in the primary and secondary pore space also allows decoupling of weighting schemes for these two flows and thus a realisation of the intended easy propagation of the dilation front according to the assumption of quick equilibration.

The modified TOUGH2 code has been applied to a hypothetical German repository for radioactive waste with non-negligible heat generation (heat transport was not simulated). In 17 alternative cases, one or two model parameters were varied against a reference case to identify sensitive parameters.

For the considered generic repository model it was found that the dilation process facilitates the escape of gas from the repository considerably. This leads to an effective limitation of gas pressures inside the repository and prevents macro-fracturing in cases where the advective flow of gas in the primary porosity is very small.

Sensitive Parameters

The dilation threshold, the capillary pressure function, the anisotropy of pressure-induced gas permeability, and the primary porosity have the strongest impact on the pressure limitation and on the volume of the dilated rock zone. The life time of the dilation zone is mainly affected by the gas generation rate and the amount of dilation.

The specific pressure-dependency of the gas permeability and secondary porosity above the dilation thresholds has no major influence on the gas migration process. The corresponding parameters are therefore judged to be not sensitive for the considered reference case. This is beneficial for the safety assessment with regard to the uncertainties connected to the experimental quantification of these parameters.

Possibly the influence of the specific pressure-dependency of the gas permeability and secondary porosity was overruled by the dominant influence of the dilation threshold decrease in upward direction. Therefore, the choice of dilation parameters might still be of importance in systems with constant dilation thresholds, e.g. in systems with horizontal propagation of the dilation zone or in small-scale systems.

Geometry of the dilation zone

In the model, a strong anisotropy of the dilation-induced gas permeability is needed to force the dilation zone to propagate in the horizontal instead of the vertical direction (bedding planes are thought to be orientated horizontally). This attributes to the fact that the minimal principal stresses decrease in upward direction. The dilation thresholds, which are connected to the minimal principal stress, therefore continuously drop at the dilation front as it moves upward through the host rock. This facilitates the propagation of the dilation zone and furthermore decreases the gas pressures inside the repository. Therefore, from the viewpoint of safety, a vertical propagation of the dilation zone is more favourable than a horizontal one.

Still, clay stone has a strong textural and mechanical anisotropy which facilitates a gas flow parallel to the bedding planes. It has to be investigated by experiments whether the mechanical anisotropy of clay stone is large enough to force a horizontal propagation of the dilation zone along the bedding planes as it was postulated by /NAG 02, 02b/ and /JOH 06/ or whether a vertical propagation will take place according to the assumptions of /BFS 05/.

It has to be noted that in the observed case of a vanishing vertical component of the additional gas flux caused by dilation (for extreme anisotropy), gas migration and pressure evolution will probably depend on the thickness of the clay layer which is subjected to dilation. The thickness of this layer does not need to correspond with the height of the repository. An estimation of this thickness is probably connected to large uncertainties.

Storage Capacity for the Gas Phase

The gas migration shows a strong dependency on the host rock's storage capacity for a gas phase. The main factors controlling the storage capacity are the primary porosity and the capillary pressure function. In all considered cases the secondary porosity gained by dilation was too small to have a significant influence on the storage capacity for a gas phase. Thus, desaturation of the primary porosity was the driving process for the storage of the gas phase. However, it has to be noted that this observation strongly depends on the capillary pressure functions that have been used. If one would assume a very rigorous threshold behaviour for gas entry into a saturated clay stone and a dilation threshold lower than the gas entry threshold there would not be any desaturation of the primary porosity and the gas phase would be stored only in the secondary porosity.

Gas Entry Pressures and Capillary Pressure Function

The importance of the capillary pressure function implies that gas migration reacts sensitive to the way gas entry pressures are introduced. As explained in chapter 5.2.6, p. 43, different relative gas permeability and capillary pressure functions can be used to introduce the same gas entry pressure. Yet, different capillary pressure functions allow different amounts of desaturation and imply different storage capacities for the gas phase. It has to be concluded that the constitutive two-phase flow relations for the capillary pressure and relative gas permeability do not only have to reflect the gas entry behaviour of the rock correctly but also have to capture the storage capacity of the rock for the gas phase. This requires accurate experimental measurements of capillary pressures at the high liquid saturations which can be expected under repository conditions in order to quantify how much desaturation is possible during the flow of the gas phase.

When desaturating the rock, the commonly used van Genuchten capillary pressure function shows an increase of the capillary pressure which is relatively slow compared to what could be expected for clay stone. The van Genuchten function might therefore overestimate the storage capacity for the gas phase and consequently underestimate the gas pressures inside the repository. The van Genuchten function, which is a quite common standard assumption, should therefore be treated with care in the context of gas migration in clay stone.

Transferability and Outlook

The results achieved in this study depend on the definition of the reference case and might not be transferable to other repository concepts or site properties, especially if repository depth, gas generation rates, two-phase flow properties and dilation properties differ significantly. Many assumptions of the considered reference case are subject to uncertainty or might be a too strong simplification of reality. Homogeneity has been assumed for the initial conditions and for the properties of the host rock. The process of resaturation of the host rock has not been considered for the definition of initial conditions and gas generation rates, which are dependent on water availability for metal corrosion. There is considerable uncertainty regarding the two-phase properties of the clay at high liquid saturations, especially with regard to the storage capability of the primary pore space for a gas phase. This storage capability might still be overestimated in the considered calculation cases. A decrease would increase the importance of gas storage in secondary pore space.

In order to substantiate the findings of this study, experimental evidence is needed regarding the anisotropy of pathway dilation in clay stone and the two-phase flow properties of clay for high liquid saturations. The proposed model still has to be qualified with respect to the physical relevance of the conceptual model. Additional consideration of mechanical interactions between stress field, flow and dilation processes might prove necessary in the future.

7 References

/BFS 05/ J. Skrzyppek, G. Mayer, St. Wilhelm, M. Niemeyer, St. Folle, O. Rolfs, D. Suter: Untersuchung der Gasbildungsmechanismen in einem Endlager für radioaktive Abfälle und der damit verbundenen Auswirkungen auf die Führung des Nachweises der Endlagersicherheit, Abschlussbericht. Colenco Bericht 3161/28, Baden, 2005.

/CAL 06/ Calder N., Avis J., Senger R., Leung H.: Modifying TOUGH2 to support modeling of gas transport through saturated compacted bentonite as part of the large-scale gas injection test (LASGIT) in Sweden, Proceedings of TOUGH Symposium 2006, Lawrence Berkeley National Laboratory, California, May 15-17, 2006.

/COR 54/ Corey, A.: The Interrelation Between Gas and Oil Relative Permeabilities, Producers Monthly, November 1954, 38-41., 1954.

/CRO 06/ J. Croisé, G. Mayer, P. Marschall, J.M. Matray, T. Tanaka, P. Vogel: Gas Threshold Pressure Test Performed at the Mont Terri Rock Laboratory (Switzerland): Experimental Data and Data Analysis. Oil & Gas Science and Technology – Rev. IFP, Vol. 61 (2006), No. 5, pp. 631-645., 2006.

/FIN 09/ S. Finsterle: iTOUGH2-IFC: An Integrated Flow Code in Support of Nagra's Probabilistic Safety Assessment. User's Guide and Model Description. Lawrence Berkeley National Laboratory, Berkley, California, 2009.

/GEN 80/ Van Genuchten, M.: A Closed-Form Equation for Predicting the Hydraulic Conductivity of Unsaturated Soils, Soil Sci. Soc.,1980, 44. 892-898., 1980.

/GRS 08/ A. Rübel, J. Mönig (eds): Gase in Endlagern im Salz, Workshop der GRS in Zusammenarbeit mit dem PTKA-WTE, Berlin, 17.-18. April 2007. Gesellschaft für Anlagen- und Reaktorsicherheit (GRS) mbH, GRS-242, 2008.

/HOC 04/ Hoch A.R., Cliffe K.A., Swift B.T., Rodwell W.R.: Modeling Gas Migration in Compacted Bentonite: Gambit Club Phase 3 Final Report, Posiva Oy, Posiva 2004-02., 2004.

/HOR 96/ Horseman, S.T., Higgo, J.J.W., Alexander, J., Harrington, J.F.: Water, gas and solute movement through argillaceous media, NEA Report CC-96/1, Paris, OECD., 1996.

/IFC 67/ International Formulation Committee: A Formulation of the Thermodynamic Properties of Ordinary Water Substance, IFC Secretariat, Diisseldorf, Germany., 1967.

/JOH 06/ L. H. Johnson, P. Zuidema: Long-term Performance Issues for Disposal Canisters for Spent Fuel and HLW in Switzerland. IHLRWM 2006, Las Vegas, NV, April 30- May 4, 2006.

/KLI 41/ Klinkenberg, L. J.: The Permeability of Porous Media to Liquids and Gases, in API Drilling and Production Practice, pp. 200-213., 1941.

/LAN 69/ Landolt-Börnstein: Zahlenwerte und Funktionen aus Physik, Chemie, Astronomie, Geophysik und Technik, sechste Auflage, IV. Band Technik, 1. Teil Stoffwerte und mechanisches Verhalten von Nichtmetallen, Berlin-Göttingen-Heidelberg, Springer Verlag., 1969.

/MAR 05/ Marschall P., Horseman S., Gimmi T.: Characterisation of Gas Transport Properties of the Opalinus Clay, a Potential Host Rock Formation for Radioactive Waste Disposal, Oil and Gas Science and Technology - Rev. IFP, Vol. 60 (2005), No. 1, pp. 121-139., 2005.

/MAZ 03/ Mazurek, M., Pearson F.J., Vockaert, G., Bock, H.: Features, Events and Processes Evaluation Catalogue for Argillaceous Media, OECD/NEA, 2003.

/NEA 01/ Nuclear Energy Agency (NEA): Gas Generation and Migration in Radioactive Waste Disposal - Workshop Proceedings, Reims, France, 26-28 June 2000. NEA, ISBN 92-64-18672-7, Paris, 190 p., 2001.

/NAG 02/ Nationale Genossenschaft für die Lagerung radioaktiver Abfälle (NAGRA): Projekt Opalinuston, Synthese der geowissenschaftlichen Untersuchungs-ergebnisse, Entsorgungsnachweis für abgebrannte Brennelemente, verglaste hochaktive sowie langlebige mittelaktive Abfälle Nagra, NTB 02-03, 2002.

/NAG 02b/ Nationale Genossenschaft für die Lagerung radioaktiver Abfälle (NAGRA): Project Opalinus Clay, Models, Codes and Data for Safety Assessment, Demonstration of disposal feasibility for spent fuel, vitrified high-level waste and long-lived intermediate-level waste (Entsorgungsnachweis), Nagra, NTB 02-06, Dez. 2002.

/NAV 08/ M. Navarro (ed.), B. Baltes, T. Beuth, G. Bracke, H. Fischer, K. Fischer-Appelt, S. Hotzel, V. Javeri, A. Kindt, L. Lambers, J. Larue, B. McStocker, U. Oppermann, E. Schrödl: Verfolgung und Bewertung der Fortentwicklung des Standes von Wissenschaft und Technik beim Nachweis der Langzeitsicherheit von Endlagern, Abschlussbericht zum Vorhaben SR 2548. Gesellschaft für Anlagen- und Reaktorsicherheit (GRS) mbH, GRS-A-3418, 2008.

/PRE 96/ William H. Press, Saul A. Teukolsky, William T. Vetterling, Brian P. Flannery, Michael Metcalf: Numerical Recipes in Fortran 90, Vol. 2., 1996.

/PRU 99/ Pruess, K., C. Oldenburg, and G. Moridis: *TOUGH2 User's Guide, Version 2.0*, Report LBNL-43134, Lawrence Berkeley National Laboratory, Berkeley, Calif., 1999.

/ROD 03/ Rodwell, W., Cool, W., Cunado, M. Johnson, L., Mäntynen, M., Müller, W., Sellin, P., Snellman, M., Talandier, J., Vieno, T., Vines, S.: A thematic network on gas issues in safety assessment of deep repositories for radioactive waste (Gasnet), Final Report, European Commission, EUR 20620EN, 45 p., 2003.

/SEN 06/ R. Senger, B. Lanyon, P. Marschall, S. Vomvoris, A. Fujiwara: TOUGH2/ITOUGH2 Analysis of the Gas Migration Test (GMT) at the Grimsel Test Site (Switzerland). Proceedings, TOUGH Symposium 2006, Lawrence Berkeley National Laboratory, Berkley, California, 2006

/SWI 01/ Swift, B.T., Hoch, A.R., Rodwell, W.R.: Modelling gas migration in compacted bentonite: GAMBIT Club Phase 2 Final Report, Posiva Oy, Posiva 2001-02, 151 p., 2001.